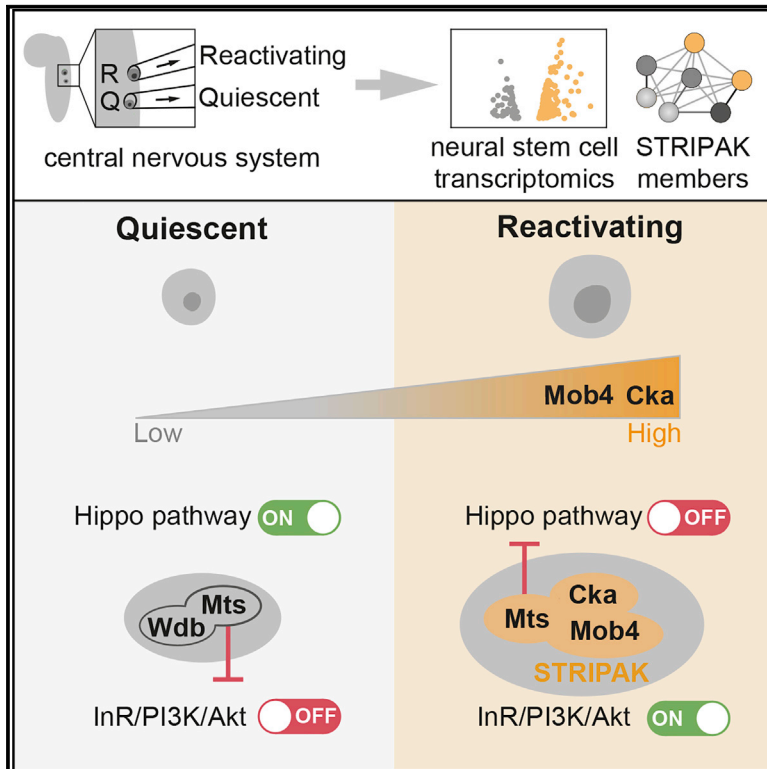


STRIPAK Members Orchestrate Hippo and Insulin Receptor Signaling to Promote Neural Stem Cell Reactivation

Graphical Abstract



Authors

Jon Gil-Ranedo, Eleanor Gonzaga, Karolina J. Jaworek, Christian Berger, Torsten Bossing, Claudia S. Barros

Correspondence

claudia.barros@plymouth.ac.uk

In Brief

The integration of signals allowing stem cell reactivation from quiescence is unclear. Gil-Ranedo et al. identify STRIPAK members Mob4, Cka, and PP2A/Mts through reactivating versus quiescent neural stem cell (NSC) transcriptional profiling. Their findings suggest that Mob4/Cka/Mts functions as an intrinsic molecular switch coordinating Hippo and InR/PI3K/Akt pathways, enabling NSC reactivation.

Highlights

- Transcriptional profiling of reactivating versus quiescent NSCs identifies STRIPAK members
- PP2A/Mts phosphatase inhibits Akt activation, maintaining NSC quiescence
- Mob4 and Cka target Mts to Hippo to inhibit its activity and promote NSC reactivation
- Mob4/Cka/Mts coordinate Hippo and InR/PI3K/Akt signaling in NSCs



STRIPAK Members Orchestrate Hippo and Insulin Receptor Signaling to Promote Neural Stem Cell Reactivation

Jon Gil-Ranedo,^{1,3} Eleanor Gonzaga,^{1,3} Karolina J. Jaworek,^{1,4} Christian Berger,^{2,5} Torsten Bossing,¹ and Claudia S. Barros^{1,6,*}

¹Faculty of Medicine and Dentistry, University of Plymouth, PL6 8BU Plymouth, UK

²Institute of Genetics, Johannes Gutenberg University, 55099 Mainz, Germany

³These authors contributed equally

⁴Present address: Living Systems Institute, University of Exeter, EX4 4QD Exeter, UK

⁵Sanofi Aventis Deutschland GmbH, 55126 Mainz, Germany

⁶Lead Contact

*Correspondence: claudia.barros@plymouth.ac.uk

<https://doi.org/10.1016/j.celrep.2019.05.023>

SUMMARY

Adult stem cells reactivate from quiescence to maintain tissue homeostasis and in response to injury. How the underlying regulatory signals are integrated is largely unknown. *Drosophila* neural stem cells (NSCs) also leave quiescence to generate adult neurons and glia, a process that is dependent on Hippo signaling inhibition and activation of the insulin-like receptor (InR)/PI3K/Akt cascade. We performed a transcriptome analysis of individual quiescent and reactivating NSCs harvested directly from *Drosophila* brains and identified the conserved STRIPAK complex members *mob4*, *cka*, and *PP2A* (*microtubule star*, *mts*). We show that PP2A/Mts phosphatase, with its regulatory subunit Widerborst, maintains NSC quiescence, preventing premature activation of InR/PI3K/Akt signaling. Conversely, an increase in Mob4 and Cka levels promotes NSC reactivation. Mob4 and Cka are essential to recruit PP2A/Mts into a complex with Hippo kinase, resulting in Hippo pathway inhibition. We propose that Mob4/Cka/Mts functions as an intrinsic molecular switch coordinating Hippo and InR/PI3K/Akt pathways and enabling NSC reactivation.

INTRODUCTION

Brain homeostasis and damage repair depend on the generation of new neurons and glia by neural stem cells (NSCs). In adult brains, most NSCs are found to be quiescent but can enter proliferation if prompted by extrinsic and intrinsic stimuli. The balance between quiescence and reactivation is critical for the maintenance of an NSC reservoir (Cavallucci et al., 2016; Chaker et al., 2016). Mechanistic insight underlying NSC quiescence and reactivation remains limited—in particular, how regulatory signals are integrated.

In the model organism *Drosophila*, embryonic NSCs give rise to the larval functional CNS. Similar to mammals, NSCs become quiescent at the end of embryogenesis and reactivate postembryonically to generate neurons and glia of the adult brain (Truman and Bate, 1988). Quiescence entry is regulated by Hox proteins, temporal transcription factors, and levels of the homeodomain transcription factor Prospero (Otsuki and Brand, 2019; Lai and Doe, 2014; Tsuji et al., 2008). NSCs are kept quiescent by the canonical Hippo pathway, whereby its core kinases Hippo and Warts prevent the transcriptional co-activator Yorkie from entering the nucleus and triggering growth (Ding et al., 2016; Poon et al., 2016). This signaling can be modulated by niche glia cells via the upstream regulators Crumbs and Echinoid, expressed in both glia and NSCs (Ding et al., 2016). NSC reactivation involves cell size increase, from 4 to 5 μm during quiescence, followed by entry into division (Ding et al., 2016; Chell and Brand, 2010; Prokop and Technau, 1991; Truman and Bate, 1988). NSCs continue to enlarge, reaching up to 10–15 μm when proliferating (Prokop and Technau, 1991; Truman and Bate, 1988). Nutrition stimulates reactivation (Britton and Edgar, 1998): dietary amino acids in the young larvae induce a systemic signal that triggers blood-brain barrier glia to secrete *Drosophila* insulin-like peptides (dILPs), a process that depends on gap junction proteins and synchronized calcium pulses (Spéder and Brand, 2014). dILPs activate the insulin-like receptor (InR)/phosphoinositide 3-kinase (PI3K)/Akt cascade in neighboring NSCs, promoting quiescence exit (Sousa-Nunes et al., 2011; Chell and Brand, 2010). The conserved heat shock protein 38/90 chaperone associates with InR to promote reactivation, and Spindle matrix proteins, including Chromator, function downstream of InR/PI3K/Akt signaling in this process (Huang and Wang, 2018; Li et al., 2017).

We performed a small-scale transcriptome analysis using single quiescent and reactivating NSC samples obtained directly from live *Drosophila* brains. Members of the evolutionary conserved striating-interacting phosphatase and kinase (STRIPAK) complex (Shi et al., 2016; Ribeiro et al., 2010) were identified and validated: monopolar spindle-one-binder family member 4 (Mob4); connector of kinase to AP-1 (Cka), which is



the sole *Drosophila* Striatin protein; and the catalytic subunit of protein phosphatase 2A (PP2A; *Drosophila* Microtubule Star [Mts]). STRIPAK contains multiple components, some of which are mutually exclusive, and STRIPAK members are part of a variety of regulatory proteins that can direct the pleiotropic PP2A to specific targets (Shi et al., 2016; Ribeiro et al., 2010; Virshup, 2000). In *Drosophila* and mammals, a STRIPAK-PP2A complex containing Mob4 and Cka was reported to inhibit Hippo signaling (Zheng et al., 2017; Couzens et al., 2013; Ribeiro et al., 2010). We show that PP2A/Mts, with its regulatory subunit Widerborst (Wdb), contributes to NSC quiescence via the inactivation of Akt, an essential component of the InR/PI3K/Akt signaling cascade. Conversely, NSC reactivation requires Mob4 and Cka, which are necessary within STRIPAK for Mts association to Hippo and subsequent Hippo pathway inhibition. These findings suggest a mechanism coordinating Hippo and InR/PI3K/Akt signaling in NSCs, enabling the transition from quiescence to proliferation.

RESULTS

Transcriptome Analysis of Reactivating NSCs: Identification of Mob4, Cka, and PP2A/Mts

To identify the mechanisms regulating NSC reactivation, we performed a small-scale analysis comparing single-cell transcriptomes of quiescent and reactivating NSCs from *Drosophila* larval brains. By combining *grh-Gal4* with *UAS-CD8-GFP* transgenic lines, cell membranes of approximately one-third of all NSCs (Chell and Brand, 2010) were specifically labeled *in vivo*. NSCs were individually harvested from 17 h after larval hatching (ALH) brains, when both quiescent (small; diameter 4–5 μm) (Ding et al., 2016; Chell and Brand, 2010) and reactivating (enlarged) cells can be easily distinguished. Of the enlarged NSCs, only non-dividing cells without any progeny were harvested. Cells were removed from the second and third thoracic segments of the ventral nerve cords (VNCs), minimizing potential differences from spatial positioning and avoiding retrieving a mix of type I and II NSCs, as the latter are absent from VNCs. Using our single-cell transcriptome protocol (Liu and Bossing, 2016; Bossing et al., 2012), cDNA from each NSC was readily obtained. Quantitative real-time PCRs confirmed that quiescent and reactivating cells expressed the NSC markers *deadpan* (*dpn*) and *asense* (*ase*), with higher levels in the latter. Single NSC transcriptomes were compared in pairs (three reactivating versus quiescent NSC pairs) on whole-genome *Drosophila* microarrays (Figure 1A). We used a limma moderated paired t test (Ritchie et al., 2015) to shortlist potential candidates, since the limited sample size did not support false discovery rate (FDR) correction. We identified 196 genes with consistent fold expression changes across all 3 replicates ($p < 0.05$), of which 145 are upregulated and 51 are downregulated (Figure 1B; Table S1; see Method Details). For quality control, we performed quantitative real-time PCR using independent single NSC samples on a subset of candidates classed mainly into *nervous system development* and *neurogenesis* Gene Ontology categories. Up- or downregulated expression for all 18 candidates tested in reactivating versus quiescent NSCs was confirmed, including *echinoid* (*ed*) and *ras homolog enriched in brain* (*rheb*), which are known to maintain NSC quies-

cence and promote reactivation, respectively (Ding et al., 2016; Sousa-Nunes et al., 2011) (Figures 1B and 1C).

Using FlyAtlas data (Chintapalli et al., 2007), we noted that our dataset ($p < 0.05$) is mostly enriched in genes expressed in the larval CNS, whereas among adult tissues, the highest enrichment is seen for genes expressed in ovaries, supporting reported gene sets associated with both NSC and germline stem cell maintenance and growth (Yan et al., 2014) (Figure S1A; Table S2). Most genes have highly conserved mouse (63%) and human orthologs (66%), and only 10% have no mammalian counterpart (Figure S1B; Table S1). When comparing the 175 mouse orthologs identified (single best matches) with transcripts found by previous studies as differentially expressed in quiescent versus activated mouse embryonic (Martynoga et al., 2013) or adult NSCs (Llorens-Bobadilla et al., 2015; Codega et al., 2014) and other stem cell types (Fukada et al., 2007; Venezia et al., 2004), we observed that the overlap is always highest (17–21 targets, 10%–12%) with any of the studies examining NSC transcriptomes (Figure S1C; Table S3). These results suggest that our small-scale single-cell transcriptome analysis generated high-quality data exposing conserved genes that are potentially involved in NSC reactivation. The analysis reveals transcripts encoding for some of the core STRIPAK complex members: *mob4* and *cka* upregulated in reactivating versus quiescent NSCs, whereas *mts*, encoding the catalytic subunit of PP2A, downregulated (Figures 1C and 1D; Table S1). STRIPAK is involved in a variety of cellular functions (Shi et al., 2016), but it has no known role in NSC reactivation. To functionally test the components identified, we focused initially on Mob4.

Loss of Mob4 Prevents NSC Reactivation

Mob4 is highly expressed in the mammalian and *Drosophila* CNS (Schulte et al., 2010; Baillat et al., 2001). After validating the differential expression of *mob4* detected in NSCs (Figure 1C), we examined its protein levels. Immunostaining of NSCs highlighted with membrane-tagged GFP and Deadpan (Dpn) together with Mob4 antibodies in 17 h ALH brains, revealed higher Mob4 levels in reactivating (enlarged) versus quiescent (small) NSCs (Figures 2A–2C). To investigate the potential function of Mob4 in NSC reactivation, we first examined *mob4* null mutants (*mob4^{EYΔL3}*, hereafter *mob4^{ΔL3}*), of which 10% survive to third-instar stages (Schulte et al., 2010). NSC (Dpn⁺) membranes labeled with anti-Discs large (Dlg) and mitosis with anti-phospho-histone H3 (pH3) antibodies enabled the scoring of size (maximum diameters) and proliferation. In newly hatched larvae (1 h ALH), no differences are detected between NSCs of *mob4* mutants and controls in either brain lobes or VNCs (Figures 2D, 2G, 2J, S2A, S2D, and S2G). All NSCs are quiescent, with the exception of four mushroom body NSCs (MbNSCs) per brain lobe that continuously proliferate from embryonic stages (Ito and Hotta, 1992). However, as early as 4 h ALH, while NSCs in controls start to enlarge, those in *mob4* mutants remain small. No NSC mitosis re-entry is detected in either group (Figures 2E, 2H, 2J, S2B, S2E, and S2G). At the end of the first-instar larval stage (24 h ALH), when many NSCs in controls are enlarged and dividing, the reduction in both NSC size and proliferation in mutants is striking, with the only mitotic NSCs corresponding to MbNSCs

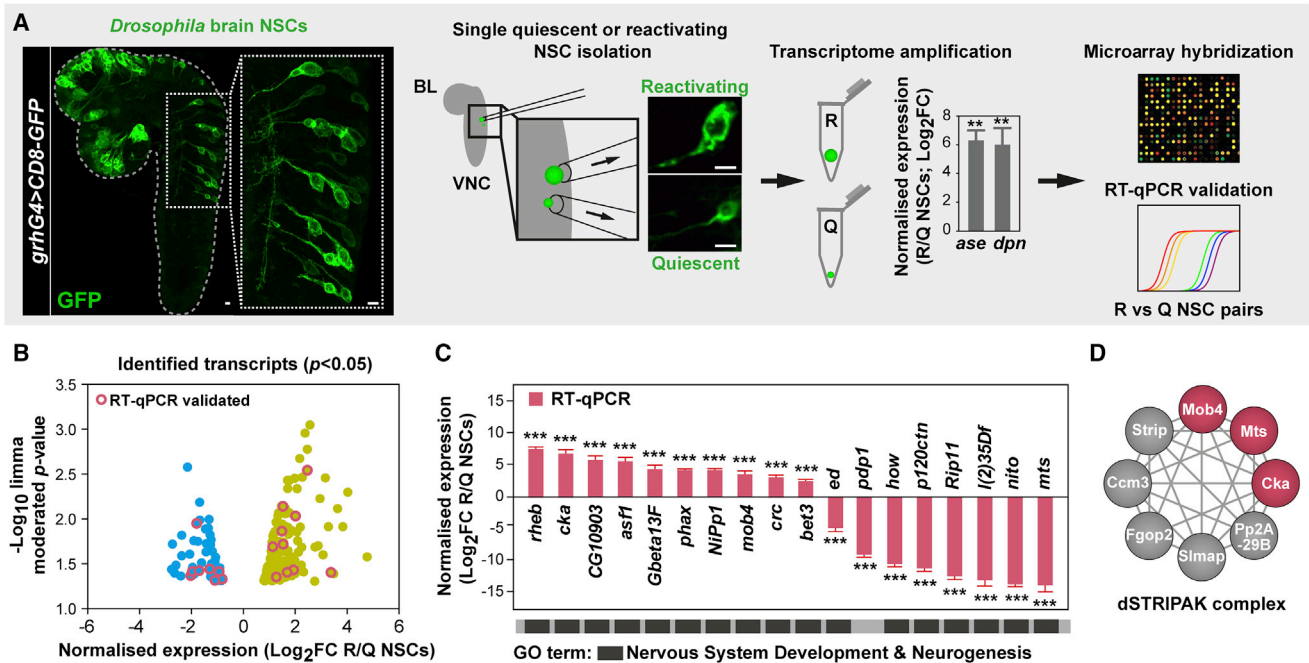


Figure 1. Single-Cell Transcriptome Analysis of Reactivating NSCs

(A) Workflow: individual quiescent (Q) and reactivating (R) NSCs expressing *CD8-GFP* driven by *grh-Gal4* were harvested from 17 h ALH CNSs, their mRNA reverse transcribed, and resulting cDNA amplified. Quantitative real-time PCRs confirmed higher *ase* and *dpn* expression in reactivating versus quiescent NSCs (normalized fold change [log₂FC]; $n = 3$ NSC reactivating/quiescent pairs; error bars: SEMs; Student's t test, $**p < 0.01$). NSC transcriptomes were compared on whole-genome microarrays (reactivating versus quiescent; three pairs) and a subset of identified targets validated by quantitative real-time PCRs. ALH, after larval hatching; BL, brain lobe; VNC, ventral nerve cord. Scale bars: 10 μ m.

(B) Distribution of identified transcripts according to average fold change expression (x axis; log₂FC) and p value (y axis; limma moderated t test; $-\log_{10}$ p value; $p < 0.05$). See also Table S1 and Figure S1.

(C) Normalized expression levels in reactivating versus quiescent NSCs obtained by quantitative real-time PCR for a subset of targets (log₂FC; $n = 3$ NSC reactivating/quiescent pairs; error bars: SEMs; Student's t test; $***p < 0.001$). The results validate the data from the microarray analysis. Most of the targets selected are classified under "nervous system development" and "neurogenesis" GO terms.

(D) STRING-based interaction network of a *Drosophila* PP2A-STRIPAK complex reported to inhibit Hippo signaling (Zheng et al., 2017; Liu et al., 2016; Ribeiro et al., 2010), highlighting (pink) the components identified in our transcriptome analysis and functionally characterized in this study.

(Figures 2F, 2I, 2J, S2C, S2F, and S2G). 5-Ethynyl-2'-deoxyuridine (EdU) incorporation assays monitoring entry into S phase confirmed that NSCs in *mob4* CNSs are not able to re-enter the cell cycle (Figures S2H–S2J). NSC reactivation defects in *mob4* mutants were similarly observed in brain lobes and VNCs. We focused subsequent studies on brain lobes.

Since niche glial cells are involved in NSC reactivation (Sousa-Nunes et al., 2011; Chell and Brand, 2010) and Mob4 is ubiquitous in the larval CNS (Schulte et al., 2010), we next tested whether Mob4 action is cell autonomous. We ectopically expressed *mob4* specifically in NSCs or in glia of *mob4* mutants using *insc-Gal4* and *repo-Gal4* drivers, respectively. NSCs were analyzed at 18 h ALH, when mitotic reactivation is ongoing. Re-introduction of Mob4 in NSCs of *mob4* mutants rescued both NSC size growth and division to the levels observed in controls (Figures 2K–2M and 2P). We observed a small increase in NSC size and division when Mob4 was expressed from glia, but levels are markedly lower than in controls (Figures 2M–2P). Finally, we inhibited Mob4 specifically in NSCs by expressing *mob4-RNAi* (Schulte et al., 2010) using *insc-Gal4*, resulting in a significant, albeit small, reduction in NSC size and a decrease

in NSC division at 18 h ALH (Figures S2K–S2M). We conclude that Mob4 functions primarily cell autonomously to promote NSC reactivation.

Overexpression of Mob4 or Its Human Ortholog Accelerates NSC Reactivation

Mob4 is highly conserved (78% identical at the amino acid level) to its human ortholog MOB4 (hMOB4, also known as Phocein), and ubiquitous expression of *hMOB4* fully rescues the lethality of *mob4* null larvae (Schulte et al., 2010). To determine whether increasing Mob4 or hMOB4 levels can promote NSC reactivation, we overexpressed these specifically in NSCs using *insc-Gal4*. Simultaneous expression of membrane-tagged GFP allowed for NSC size examination, and divisions were labeled with p3 antibodies. At 6 h ALH, NSCs in controls have yet to re-enter mitosis. At this stage, Mob4 or hMOB4 overexpression results in a premature NSC size increase. No re-entry into division was seen upon Mob4 overexpression, but hMOB4 induced a minor but significant increase (Figures 3A–3C and 3G). At 18 h ALH, no difference in NSC size was detected upon Mob4 overexpression, but more NSCs were found in mitosis compared to

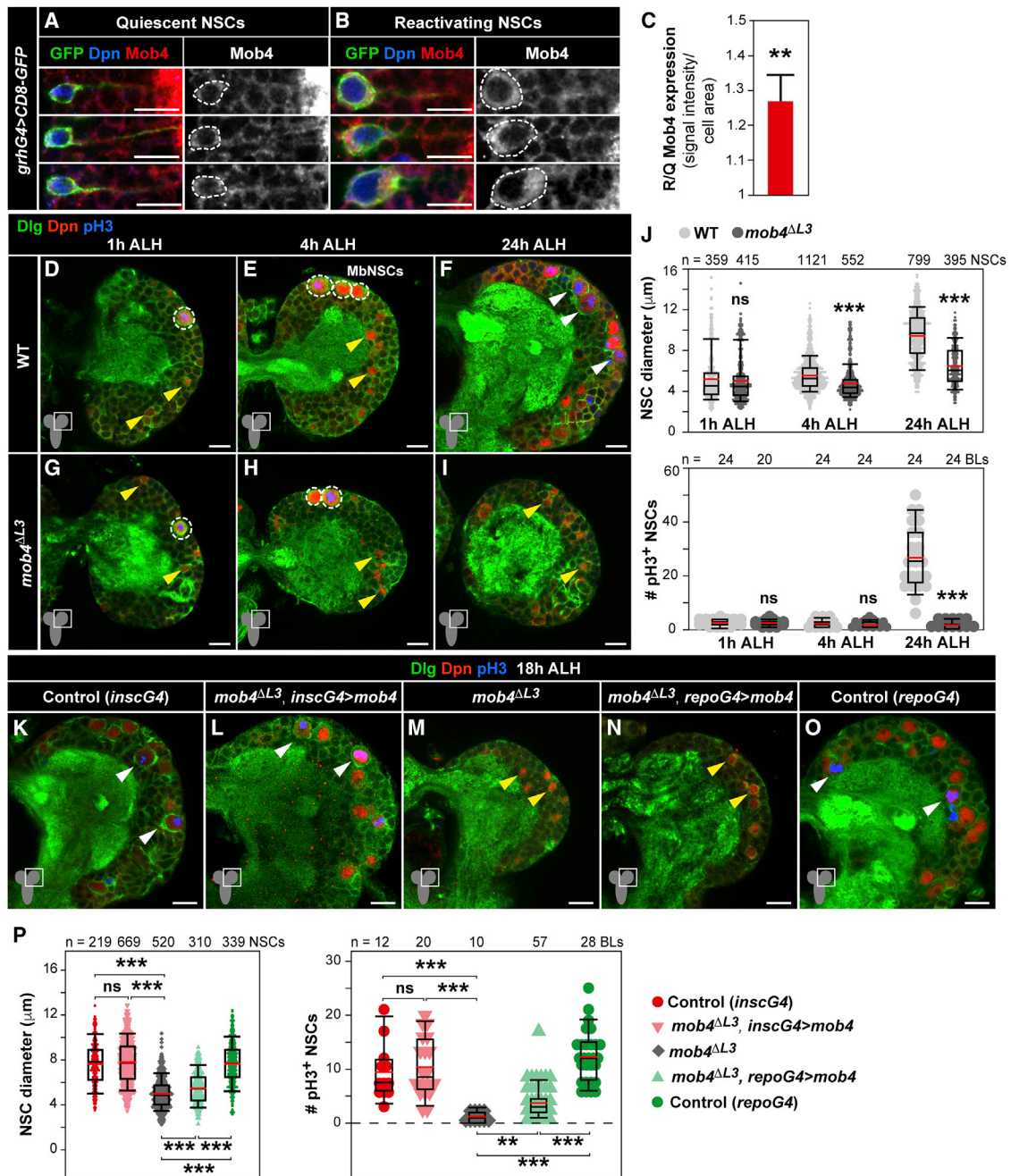


Figure 2. Loss of Mob4 Prevents NSC Mitotic Reactivation

(A–C) Mob4 is upregulated in reactivating versus quiescent NSCs. Examples of quiescent (small, A) and reactivating (enlarged, B) NSCs in 17 h ALH CNSs (VNC thoracic region) labeled with *grh-Gal4* driving *CD8-GFP* (GFP, green), Mob4 (red), and Dpn (blue). Mob4 channel also shown in monochrome. Dashed lines: cell bodies. (C) Mob4 protein quantification in reactivating normalized to quiescent NSCs (reactivating NSCs: n = 50, 8 BLs, 8 brains; quiescent NSCs: n = 50, 8 BLs, 8 brains; error bars: SEMs).

(D–J) NSC enlargement and division are impaired in *mob4*^{ΔL3} mutants. Wild-type (WT; D, 1 h ALH; E, 4 h ALH; F, 24 h ALH) and *mob4*^{ΔL3} brain lobes (G, 1 h ALH; H, 4 h ALH; I, 24 h ALH). NSCs (Dpn, red), cell membranes (Dig, green), and divisions (pH3, blue). Yellow arrowheads: quiescent NSCs; white arrowheads: reactivated NSCs. Mushroom body NSCs (MbNSCs; dashed circles) are large and do not enter quiescence. At 1 and 4 h ALH, there are no NSC divisions, except in MbNSCs.

(J) Quantification of NSC diameters (1 h ALH: WT n = 359 NSCs, 10 BLs, 5 brains; *mob4*^{ΔL3} n = 415 NSCs, 10 BLs, 7 brains; 4 h ALH: WT n = 1,121 NSCs, 14 BLs, 7 brains; *mob4*^{ΔL3} n = 552 NSCs, 10 BLs, 5 brains; 24 h ALH: WT n = 799 NSCs, 10 BLs, 7 brains; *mob4*^{ΔL3} n = 395 NSCs, 18 BLs, 9 brains) and proliferation (1 h ALH: WT n = 24 BLs, 12 brains; *mob4*^{ΔL3} n = 20 BLs, 12 brains; 4 h ALH: WT n = 24 BLs, 12 brains; *mob4*^{ΔL3} n = 24 BLs, 12 brains; 24 h ALH: WT n = 24 BLs, 12 brains; *mob4*^{ΔL3} n = 24 BLs, 12 brains).

(legend continued on next page)

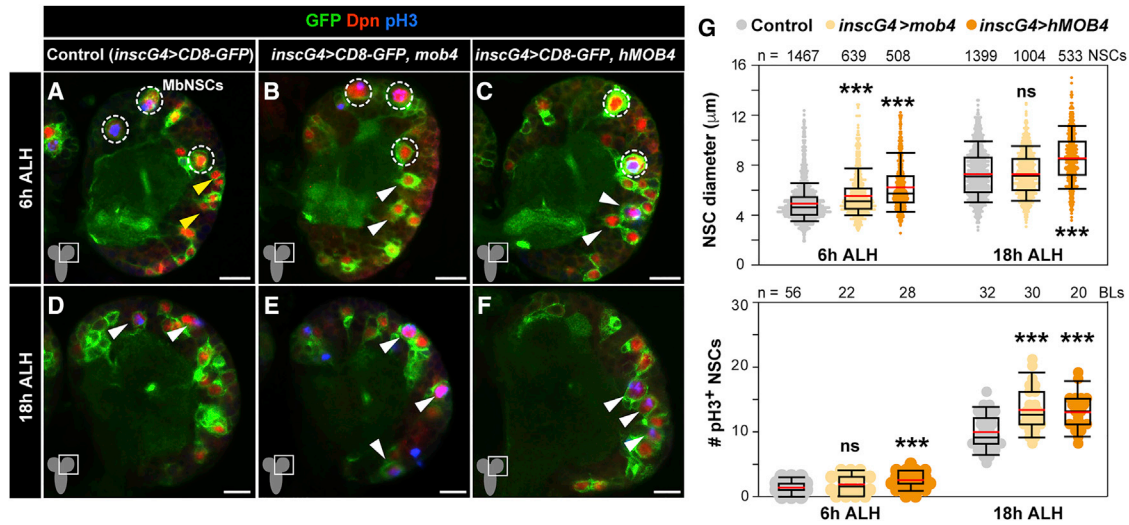


Figure 3. Overexpression of Mob4 or hMOB4 Increases NSC Growth and Division

(A–G) NSC-specific *mob4* or human *MOB4* (*hMOB4*) overexpression leads to premature NSC enlargement and mitosis entry. Brain lobes of control (A and D, *insc-gal4 > CD8-GFP*) and *mob4* (B and E, *insc-gal4 > CD8-GFP, mob4*) or *hMOB4* (C and F, *insc-gal4 > CD8-GFP, hMOB4*) overexpressing brains at 6 and 18 h ALH. NSCs in green (GFP) and red (Dpn), and divisions in blue (pH3). Dashed circles: MbNSCs; yellow arrowheads: quiescent NSC examples; white arrowheads: prematurely enlarging (B and C) and dividing NSC examples (D–F). Anterior up. Scale bars: 10 μ m.

(G) Quantification of NSC diameters (6 h ALH: *insc-gal4 > CD8-GFP* n = 1,467 NSCs, 20 BLs, 15 brains; *insc-gal4 > CD8-GFP, mob4* n = 639 NSCs, 10 BLs, 5 brains; *insc-gal4 > CD8-GFP, hMOB4* n = 508 NSCs, 7 BLs, 5 brains; 18 h ALH: *insc-gal4 > CD8-GFP* n = 1,399 NSCs, 18 BLs, 15 brains; *insc-gal4 > CD8-GFP, mob4* n = 1,004 NSCs, 13 BLs, 9 brains; *insc-gal4 > CD8-GFP, hMOB4* n = 533 NSCs, 7 BLs, 5 brains) and proliferation (6 h ALH: *insc-gal4 > CD8-GFP* n = 56 BLs, 28 brains; *insc-gal4 > CD8-GFP, mob4* n = 22 BLs, 11 brains; *insc-gal4 > CD8-GFP, hMOB4* n = 28 BLs, 14 brains; 18 h ALH: *insc-gal4 > CD8-GFP* n = 32 BLs, 16 brains; *insc-gal4 > CD8-GFP, mob4* n = 30 BLs, 15 brains; *insc-gal4 > CD8-GFP, hMOB4* n = 20 BLs, 10 brains).

Wilcoxon rank-sum tests; ***p < 0.001; p > 0.05: ns.

See also Figure S3.

controls. *hMOB4* ectopic expression increased NSC size and induced a similar increase in the number of dividing NSCs as seen upon *Mob4* overexpression (Figures 3D–3G). We next tested whether *Mob4* overexpression leads to NSC overproliferation. Scoring of NSC divisions in late larval brain lobes (94 h ALH) revealed no differences from controls, indicating that *Mob4* overexpression effects are restricted to the NSC reactivation process (Figures S3A–S3C). Finally, since NSC reactivation depends on nutritional stimulus (Britton and Edgar, 1998), we inquired as to whether *Mob4* overexpression in NSCs could induce reactivation under diet-restriction conditions. In larvae reared in the absence of dietary amino acids, NSCs overexpressing *Mob4* remained quiescent (Figures S3D–S3F). We conclude that increased *Mob4* levels accelerate NSC reactivation, and this function may be evolutionary conserved. Yet, *Mob4* is not sufficient to bypass the extrinsic nutrition stimulus required for NSC reactivation.

Mob4 Regulates InR/PI3K/Akt and Hippo Signaling Activity in NSCs

The Hippo pathway maintains NSCs in quiescence (Ding et al., 2016; Poon et al., 2016), whereas activation of InR/PI3K/Akt signaling cascade triggers reactivation (Sousa-Nunes et al., 2011; Chell and Brand, 2010). To assess how *Mob4* function relates to both pathways, we first examined their activity in the absence of *Mob4*. Upon activation, insulin receptors recruit PI3K to the cell membrane to convert phosphoinositol(4,5)P2 (PIP2) into phosphoinositol(3,4,5)P3 (PIP3), which in turn recruits the Akt protein kinase through its pleckstrin homology (PH) domain, becoming activated by phosphorylation. This process can be monitored using a PH domain-GFP fusion protein (PH-GFP) binding PIP3 (Britton et al., 2002). We confirmed strong membrane-bound accumulation of PH-GFP in reactivated NSCs (Figures 4A and 4A') (Chell and Brand, 2010). In contrast, NSCs in *mob4* mutants show weak and diffused PH-GFP signals

(K–P) *Mob4* expression in NSCs, but not in glia, rescues NSC reactivation in *mob4 Δ L3* mutants to control levels. Brain lobes of control (K, *insc-gal4*), *mob4 Δ L3* expressing *Mob4* in NSCs (L, *mob4 Δ L3, insc-gal4 > mob4*), *mob4 Δ L3* (M), *mob4 Δ L3* expressing *Mob4* in glia (N, *mob4 Δ L3, repo-gal4 > mob4*), and control (O, *repo-gal4*) at 18 h ALH.

(P) Quantification of NSC diameters (*insc-gal4* n = 219 NSCs, 3 BLs, 3 brains; *mob4 Δ L3, insc-gal4 > mob4* n = 669, 10 BLs, 5 brains; *mob4 Δ L3* n = 520 NSCs, 7 BLs, 7 brains; *mob4 Δ L3, repo-gal4 > mob4* n = 310 NSCs, 6 BLs, 6 brains; *repo-gal4* n = 339, 5 BLs, 5 brains) and proliferation (*insc-gal4* n = 12 BLs, 12 brains; *mob4 Δ L3, insc-gal4 > mob4* n = 20 BLs, 10 brains; *mob4 Δ L3* n = 10 BLs, 10 brains; *mob4 Δ L3, repo-gal4 > mob4* n = 57 BLs, 29 brains; *repo-gal4* n = 28 BLs, 14 brains) at 18 h ALH.

Wilcoxon rank-sum tests; **p < 0.01, ***p < 0.001; p > 0.05: non-significant (ns). BLs, brain lobes. Anterior up. Scale bars: 10 μ m.

See also Figure S2.

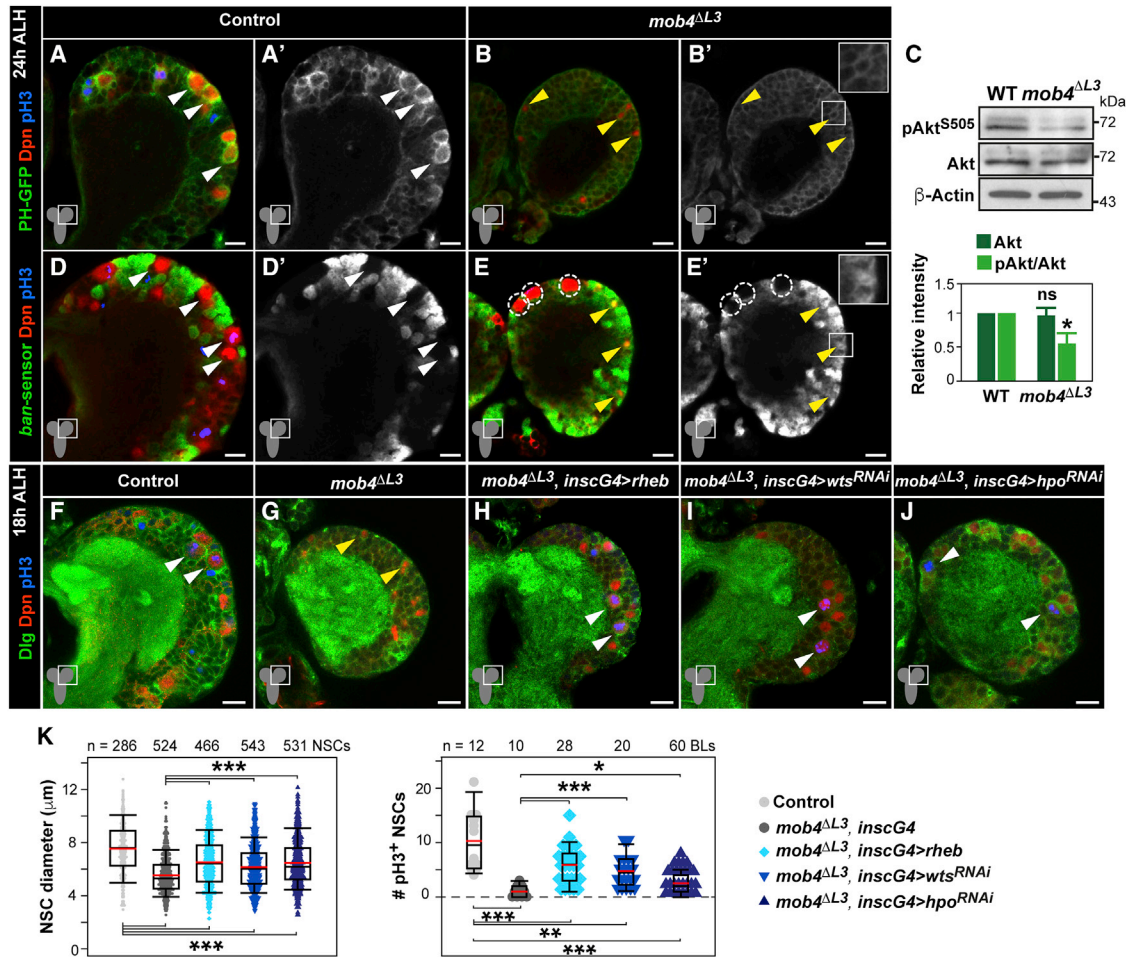


Figure 4. InR/PI3K/Akt Pathway Activation or Hippo Signaling Inhibition Rescues NSC Reactivation in *mob4* Mutants

(A–C) InR/PI3K/Akt signaling is strongly reduced in *mob4* NSCs. Expression of pleckstrin homology (PH) domain-GFP fusion (GFP, green) does not accumulate at NSC membranes of *mob4* mutants as in controls. Brain lobes of control (A) and *mob4*^{ΔL3} mutants (B) at 24 h ALH. NSCs in red (Dpn) and divisions in blue (pH3). GFP channel also shown in monochrome (A' and B'). Inset displays higher magnification (B'). Yellow arrowheads: quiescent NSC examples; white arrowheads: reactivated NSC examples.

(C) Phospho-Akt (pAkt^{S505}) is reduced in *mob4* mutant brains, while total Akt levels are comparable to those in controls (24 h ALH brain extracts; β-actin: loading control). Quantification of protein signals (bottom; error bars: SEMs; n = 3 independent assays; Student's t tests; *p < 0.05; p > 0.05: ns).

(D–E') Hippo signaling remains active in *mob4* NSCs. In contrast to controls, NSCs in *mob4* mutants show no *ban* activity, except in MbNSCs (dashed circles). *ban*-activity sensor, in which decreased GFP signal (green) reflects increased *ban* activity, in brain lobes of control (D and D') and *mob4*^{ΔL3} mutants (E and E') at 24 h ALH. NSCs in red (Dpn) and divisions in blue (pH3). GFP channel also shown in monochrome (D' and E'). Inset showing higher magnification (E').

(F–K) NSC-specific expression of *rheb* activating InR/PI3K/Akt signaling and of *warts* (*wts*)-RNAi or *hippo* (*hpo*)-RNAi inactivating Hippo signaling can rescue NSC reactivation in *mob4* mutants. Brain lobes of control (F, *insc-gal4*), *mob4*^{ΔL3} (G), *mob4*^{ΔL3} expressing *rheb* in NSCs (H, *mob4*^{ΔL3}, *insc-gal4* > *rheb*), *mob4*^{ΔL3} expressing *wts*-RNAi in NSCs (I, *mob4*^{ΔL3}, *insc-gal4* > *wts*^{RNAi}), and *mob4*^{ΔL3} expressing *hpo*-RNAi in NSCs (J, *mob4*^{ΔL3}, *insc-gal4* > *hpo*^{RNAi}) at 18 h ALH. NSCs in red (Dpn), cell membranes in green (Dlg), and divisions in blue (pH3). Anterior up. Scale bars: 10 μm and 17 μm in insets.

(K) Quantification of NSC diameters (*insc-gal4* n = 286 NSCs, 4 BLs, 3 brains; *mob4*^{ΔL3} n = 524 NSCs, 7 BLs, 7 brains; *mob4*^{ΔL3}, *insc-gal4* > *rheb* n = 466 NSCs, 6 BLs, 5 brains; *mob4*^{ΔL3}, *insc-gal4* > *wts*^{RNAi} n = 543 NSCs, 8 BLs, 5 brains; *mob4*^{ΔL3}, *insc-gal4* > *hpo*^{RNAi} n = 531 NSCs, 8 BLs, 5 brains) and divisions (*insc-gal4* n = 12 BLs, 12 brains; *mob4*^{ΔL3} n = 10 BLs, 10 brains; *mob4*^{ΔL3}, *insc-gal4* > *rheb* n = 28 BLs, 14 brains; *mob4*^{ΔL3}, *insc-gal4* > *wts*^{RNAi} n = 20 BLs, 10 brains; *mob4*^{ΔL3}, *insc-gal4* > *hpo*^{RNAi} n = 60 BLs, 30 brains).

Wilcoxon rank-sum tests; *p < 0.05, **p < 0.01, ***p < 0.001.

(Figures 4B and 4B'). We also observed reduced phosphorylated Akt levels in *mob4* whole CNS lysates compared to controls, whereas total Akt levels were equivalent (Figure 4C). To examine Hippo signaling, we tested the activity of *bantam* (*ban*) microRNA that promotes NSC size growth and division (Ding et al., 2016). In quiescent NSCs, active Hippo signaling prevents *ban* transcrip-

tion (Ding et al., 2016). We used a *ban* GFP-sensor system, in which GFP signal reduction reflects an increase in *ban* activity (Brennecke et al., 2003). No GFP is observed in control reactivated NSCs demonstrating *ban* activity (Ding et al., 2016) (Figures 4D and 4D'). However, the GFP signal is detected in the NSCs of *mob4* mutants, indicating the absence of *ban* activity

and Hippo pathway activation (Figures 4E and 4E'). We next tested whether activating InR/PI3K/Akt cascade or inhibiting Hippo pathways in the NSCs of *mob4* mutants could rescue reactivation defects. Stimulation of target of rapamycin (TOR) signaling by Rheb overexpression activates the InR/PI3K/Akt cascade, promoting premature NSC exit from quiescence (Li et al., 2017; Sousa-Nunes et al., 2011). Overexpressing Rheb in the NSCs of *mob4* mutants led to NSC size increase and division re-entry (Figures 4F–4H, and 4K). To inhibit Hippo signaling, we used RNAi against *warts* (*wts*) or *hippo*, which induce earlier NSC reactivation (Ding et al., 2016). In *mob4* brains, expression of *wts*-RNAi or *hippo*-RNAi in NSCs induced cell size growth and mitosis re-entry (Figures 4F, 4G, and 4I–4K). We conclude that the InR/PI3K/Akt signaling cascade is inhibited, while the Hippo pathway stays active in NSCs upon the loss of Mob4, consistent with NSCs in *mob4* mutants being unable to exit quiescence. Activation of InR/PI3K/Akt or inhibition of Hippo pathways can restore reactivation. However, the rescues are partial, with the NSC size and proliferation increase observed in *mob4* mutant brains not reaching control levels (Figures 4F–4K). The results contrast with the effect of expressing *rheb*, *hippo*-RNAi, or *wts*-RNAi in a control background, where NSC growth and division surpass control levels (Li et al., 2017; Ding et al., 2016; Sousa-Nunes et al., 2011) and may also reflect insufficient activation or inactivation of the respective signals and/or regulation of both pathways that are essential for effective NSC reactivation.

Mob4 and Cka Cooperate to Reactivate NSCs and Assemble a PP2A-Hippo Complex

Our analysis of single NSC transcriptomes also identified the STRIPAK scaffold protein Cka, which is expressed throughout the CNS (Shi et al., 2016; Chen et al., 2002). Similar to Mob4, we found *cka* transcript and protein upregulated in reactivating versus quiescent NSCs (Figures 1C and S4A–S4C). To examine its function, we overexpressed Cka specifically in NSCs and observed premature NSC enlargement at 6 h ALH (Figures 5A, 5B, and 5G), as well as increased NSC size and divisions at 18 h ALH (Figures 5D, 5E, and 5G). Conversely, the expression of *cka*-RNAi resulted in a small but significant reduction in NSC size and decreased NSC mitosis at 18 h ALH (Figures S4D–S4F). Next, we simultaneously overexpressed Mob4 and Cka in NSCs and observed stronger effects compared to those upon single Mob4 or Cka overexpression (Figures 5A–5G; see also Figures 3B, 3E, and 3G).

STRIPAK negatively regulates Hippo signaling via the dephosphorylation of Hippo kinase by PP2A phosphatase (Couzens et al., 2013; Ribeiro et al., 2010). We examined whether the STRIPAK components Mob4 and Cka are essential for mediating the association of PP2A to Hippo. Co-immunoprecipitations (coIPs) were conducted on S2R⁺ cell lysates expressing FLAG-tagged Hippo or control FLAG-NTAN, plus Myc-tagged Mts. In addition, we performed RNAi targeting *mob4* and/or *cka*, which effectively depletes the respective proteins (Figure S5A), using RNAi as a control against *DsRed* targeting red fluorescent protein. FLAG-Hippo co-immunoprecipitates Myc-Mts, as reported (Ribeiro et al., 2010), and no association is found with FLAG-NTAN. However, depletion of Mob4, Cka, or both impairs

Hippo/Mts binding, with the latter nearly abolishing association (Figures 5H and 5I). We verified that the inhibition of Mob4 and Cka results in increased Hippo activation, as reported (Zheng et al., 2017; Ribeiro et al., 2010), and that chemical inhibition of PP2A with okadaic acid targeting PP2A, and to a lesser extent PP1 (Takai et al., 1992), leads to Hippo hyperphosphorylation as a positive control (Figure S5B). We conclude that Mob4 and Cka cooperate to promote NSC reactivation and are both required for the association of PP2A to Hippo, leading to its inactivation, which is consistent with the Hippo pathway remaining active in NSCs upon *mob4* loss (Figures 4D–4E').

PP2A Inactivates Akt Independently of STRIPAK Cka and Mob4 Members and Maintains Quiescent NSCs

If PP2A/Mts would only function in NSCs to inactivate Hippo signaling via STRIPAK, then a prolonged NSC quiescence could be anticipated upon Mts inhibition. However, PP2A is also a well-established negative regulator of the insulin receptor signaling cascade, including by the dephosphorylation of Akt (Padmanabhan et al., 2009; Vereshchagina et al., 2008; Janssens and Goris, 2001). Using S2R⁺ cells, we observed that Mts inhibition with okadaic acid increases Akt phosphorylation, regardless of RNAi-mediated depletion of *cka* and *mob4* (Figure S6A). In addition, in S2R⁺ cells expressing hemagglutinin (HA)-tagged Mts and Myc-tagged Akt, Mts co-immunoprecipitates with Akt. However, unlike for Mts/Hippo interaction, the depletion of *cka* and *mob4* does not disturb Mts/Akt association, nor does it disturb the levels of phosphorylated Akt with or without insulin stimulation (Figures S6A–S6C). Next, we examined whether impaired Mts function affects NSC reactivation. Since *mts* null mutants (*mts*^{XE-2258}) are embryonic lethal (Snaith et al., 1996), we analyzed transheterozygotes harboring an *mts* hypomorphic allele surviving to pupal stages (*mts*²⁹⁹) (Wang et al., 2009) and *mts*^{XE-2258}. Reactivating NSCs in *mts*²⁹⁹/*mts*^{XE-2258} mutants shows a mild increased cell size as compared to controls (Figures 6A–6C). To knock down *mts* specifically in NSCs, we expressed a dominant-negative *mts* mutant (*mts*-DN) lacking the N-terminal region of the phosphatase domain (Hannus et al., 2002). Premature NSC size increase and entry into division were observed (Figures 6D, 6E, 6G, 6H, and 6J), strengthening the results using *mts* transheterozygotes. We then examined whether the regulatory PP2A subunit Wdb, shown to modulate Akt downstream of InR/PI3K/Akt signaling in both vertebrates and invertebrates (Rodgers et al., 2011; Padmanabhan et al., 2009; Vereshchagina et al., 2008), may also function in NSCs. Similar to *mts*-DN, expression of a truncated *wdb* mutant form acting as a dominant negative (*wdb*-DN) (Hannus et al., 2002) leads to increased NSC size growth at 6 h ALH and a higher number of mitotic NSCs at 18 h ALH (Figures 6D, 6F, 6G, 6I, and 6J). Next, we ascertained whether PP2A/Mts inhibition affects pAkt levels. A premature increase in pAkt is seen in NSCs expressing *mts*-DN, which indicates abnormal InR/PI3K/Akt activation (Figures 6K–6L'). In this condition, a moderate but significant reduction of *ban* activity (indicated by *ban*-GFP sensor signal increase) is also observed (Figures 6M–6O). The results suggest that the inhibition of Mts can promote Hippo signaling activity in NSCs, but the effect is insufficient, possibly due to the availability of endogenous Mob4/Cka levels at this stage, or otherwise

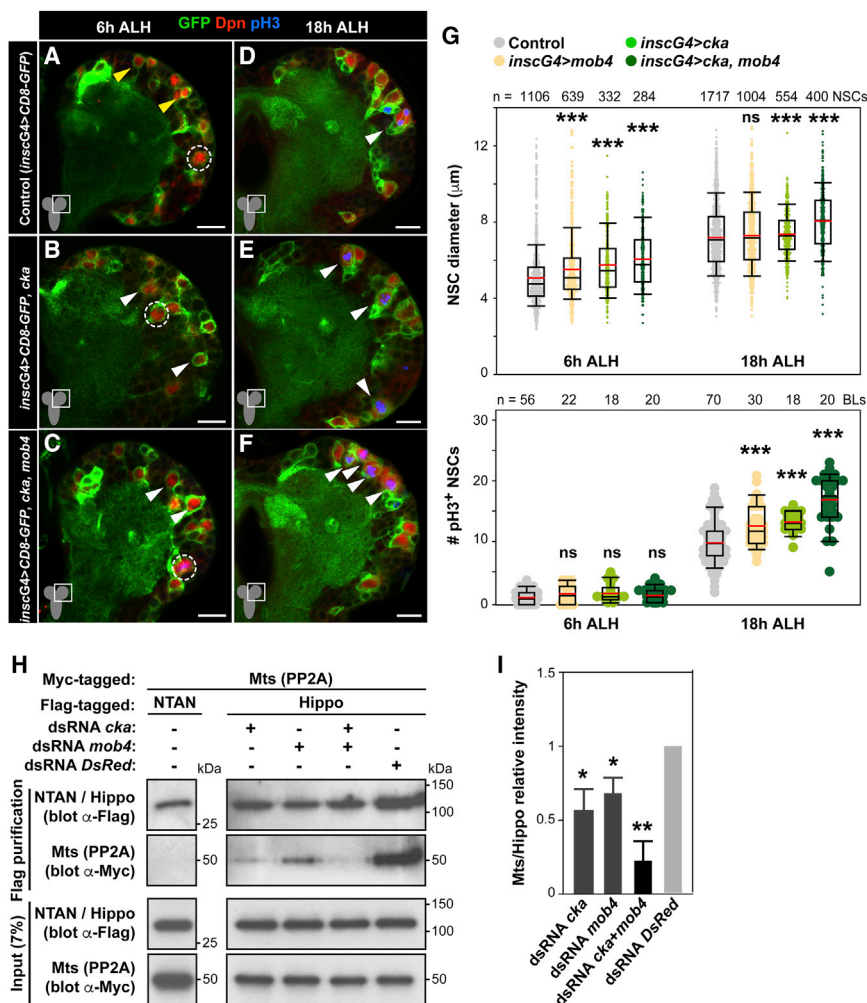


Figure 5. Cka and Mob4 Cooperate to Promote NSC Reactivation and Are Required for PP2A/Hippo Interaction

(A–G) NSC-specific *cka* or *cka* and *mob4* double overexpression leads to premature enlargement and increased mitotic NSCs. Double overexpression results in stronger effects (see also Figure 3). Brain lobes of control (A and D, *inscGal4 > CD8-GFP*), *cka* (B and E, *inscGal4 > CD8-GFP, cka*), and double *cka* and *mob4* (C and F, *inscGal4 > CD8-GFP, cka, mob4*) overexpressing brains at 6 and 18 h ALH. NSCs in green (GFP) and red (Dpn), and divisions in blue (pH3). Dashed circles: MbNSCs; yellow arrowheads: quiescent NSCs; white arrowheads: prematurely enlarging (B and C) and dividing NSCs (D–F). Anterior up. Scale bars: 10 μ m.

(G) Quantification of NSC diameters (6 h ALH: *inscGal4 > CD8-GFP* n = 1,106 NSCs, 15 BLs, 10 brains; *inscGal4 > CD8-GFP, mob4* n = 639 NSCs, 10 BLs, 5 brains; *inscGal4 > CD8-GFP, cka* n = 332 NSCs, 5 BLs, 5 brains; *inscGal4 > CD8-GFP, cka, mob4* n = 284 NSCs, 8 BLs, 8 brains; 18 h ALH: *inscGal4 > CD8-GFP* n = 1,717 NSCs, 19 BLs, 14 brains; *inscGal4 > CD8-GFP, mob4* n = 1,004 NSCs, 13 BLs, 9 brains; *inscGal4 > CD8-GFP, cka* n = 554 NSCs, 8 BLs, 4 brains; *inscGal4 > CD8-GFP, cka, mob4* n = 400 NSCs, 6 BLs, 4 brains) and divisions (6 h ALH: *inscGal4 > CD8-GFP* n = 56 BLs, 28 brains; *inscGal4 > CD8-GFP, mob4* n = 22 BLs, 11 brains; *inscGal4 > CD8-GFP, cka* n = 18 BLs, 9 brains; *inscGal4 > CD8-GFP, cka, mob4* n = 20 BLs, 10 brains; 18 h ALH: *inscGal4 > CD8-GFP* n = 70 BLs, 38 brains; *inscGal4 > CD8-GFP, mob4* n = 30 BLs, 15 brains; *inscGal4 > CD8-GFP, cka* n = 18 BLs, 9 brains; *inscGal4 > CD8-GFP, cka, mob4* n = 20 BLs, 10 brains). Wilcoxon rank-sum tests, ***p < 0.001; p > 0.05: ns. See also Figure S4.

(H and I) Depletion of Mob4 and/or Cka inhibits PP2A/Mts association to Hippo.

(H) CoIP assays using S2R⁺ cells expressing Myc-Mts and FLAG-Hippo or control FLAG-NTAN, in addition to RNAi against *mob4* and/or *cka* or control *DsRed* (see also Figure S5). Lysates and FLAG-purified immunoprecipitates analyzed by western blot with indicated antibodies.

(I) Quantification of relative binding of Myc-Mts to FLAG-Hippo shown as a mean of the ratio between Myc-Mts and FLAG-Hippo signal intensities relative to control (*DsRed* RNAi) levels (n = 3 independent assays; error bars: SEMs; Student's t tests; *p < 0.05 and **p < 0.01).

dominated by InR/PI3K/AKT activation, with the final outcome being premature NSC reactivation. Our data indicate that PP2A/Mts may play a dual role in early postembryonic NSCs: first with Wdb to target Akt contributing to quiescence maintenance and second with STRIPAK components Mob4 and Cka targeting Hippo signaling to promote reactivation (Figure 6P).

DISCUSSION

Neural replenishment depends on the ability of NSCs to tightly control the balance between quiescence and proliferation (Tian et al., 2018; Chaker et al., 2016; Cheung and Rando, 2013). Recent advances in profiling quiescent and activated NSCs are increasing our understanding of these cell states. Most approaches have relied on brain tissue dissociation, cell sorting, and culturing procedures (Llorens-Bobadilla et al., 2015; Codega et al., 2014; Martynoga et al., 2013). Here, we reveal a transcript profile of single quiescent versus reactivating NSC samples

obtained directly from live brains. The analysis of identified individual cells taken directly from living tissues at desired time points allows us to precisely examine the transcriptional control at the crossroads of crucial cell fates. Due likely to the reduced sample number and single-cell cDNA amplification variability (Tung et al., 2017; Macaulay and Voet, 2014) (Pearson's r correlations obtained: quiescent NSCs 0.75 < r < 0.81, mean: 0.77; reactivating NSCs 0.58 < r < 0.67, mean: 0.61), our analysis did not support FDR correction. However, the identified genes meeting significance (limma moderated t test, p < 0.05) show consistent expression changes across replicates, and the regulation of all of the targets tested was independently validated. The high conservation with mammalian genes and partial overlap with orthologs reported to be differentially expressed in mouse quiescent versus activated NSCs suggest that our dataset is also a valuable resource for mammalian NSC research.

Adult NSCs must orchestrate extrinsic signals according to the organism's status with intrinsic factors to transit between

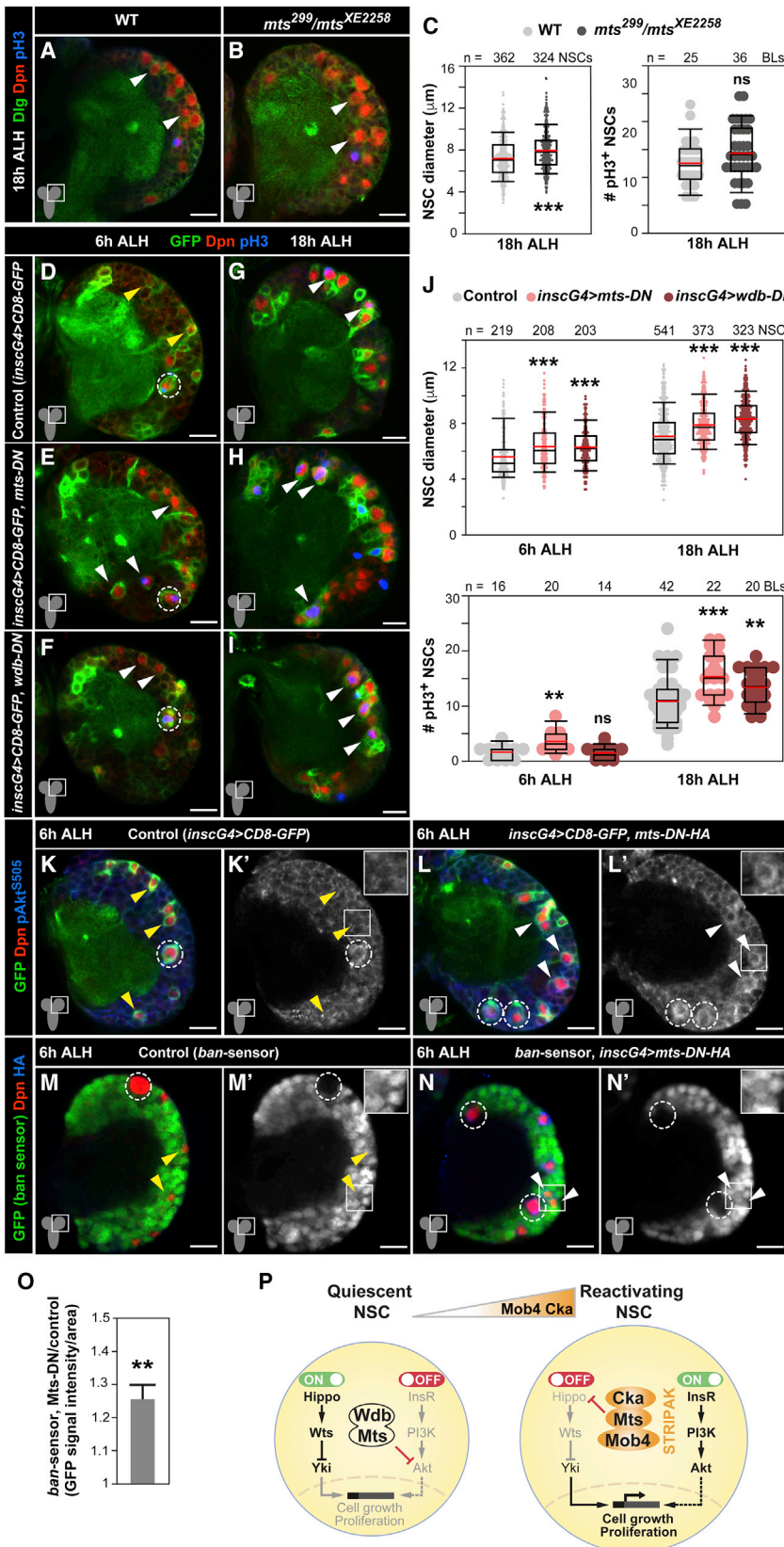


Figure 6. Inactivation of PP2A Phosphatase Results in Premature NSC Reactivation

(A–C) *PP2A/mts* hypomorphic mutants show premature NSC size growth. Brain lobes of WT (A) and *mts²⁹⁹/mts^{XE2258}* mutants (B) at 18 h ALH. NSCs in red (Dpn), cell membranes in green (Dig), and divisions in blue (pH3). Arrowheads: NSC examples.

(C) Quantification of NSC diameters (WT n = 362 NSCs, 5 BLs, 3 brains; *mts²⁹⁹/mts^{XE2258}* n = 324 NSCs, 6 BLs, 5 brains) and divisions (WT n = 25 BLs, 13 brains; *mts²⁹⁹/mts^{XE2258}* n = 36 BLs, 27 brains). Wilcoxon rank-sum tests; ***p < 0.001; p > 0.05: ns.

(D–J) NSC-specific expression of dominant-negative (DN) forms of PP2A catalytic subunit Mts or regulatory subunit Wdb results in premature NSC size growth and an increased number of mitotically reactivated NSCs. Brain lobes of control (D and G, *insc-gal4* > *CD8-GFP*), *mts-DN* (E and H, *insc-gal4* > *CD8-GFP*, *mts-DN*), and *wdb-DN* (F and I, *insc-gal4* > *CD8-GFP*, *wdb-DN*) expressing brains at 6 and 18 h ALH. NSC in green (GFP) and red (Dpn), and divisions in blue (pH3). Dashed circles: MbNSCs; yellow arrowheads: quiescent NSC examples; white arrowheads: prematurely enlarging (E and F) and mitotically reactivated NSCs (G–I).

(J) Quantification of NSC diameters (6 h ALH: *insc-gal4* > *CD8-GFP* n = 219 NSCs, 5 BLs, 5 brains; *insc-gal4* > *wdb-DN* n = 208 NSCs, 5 BLs, 5 brains; *insc-gal4* > *mts-DN* n = 203 NSCs, 5 BLs, 5 brains; 18 h ALH: *insc-gal4* > *CD8-GFP* n = 541 NSCs, 8 BLs, 5 brains; *insc-gal4* > *CD8-GFP*, *wdb-DN* n = 373 NSCs, 5 BLs, 5 brains; *insc-gal4* > *CD8-GFP*, *mts-DN* n = 323 NSCs, 5 BLs, 5 brains) and divisions (6 h ALH: *insc-gal4* > *CD8-GFP* n = 16 BLs, 8 brains; *insc-gal4* > *CD8-GFP*, *wdb-DN* n = 20 BLs, 10 brains; *insc-gal4* > *CD8-GFP*, *mts-DN* n = 14 BLs, 7 brains; 18 h ALH: *insc-gal4* > *CD8-GFP* n = 42 BLs, 21 brains; *insc-gal4* > *CD8-GFP*, *wdb-DN* n = 22 BLs, 12 brains; *insc-gal4* > *CD8-GFP*, *mts-DN* n = 20 BLs, 10 brains). Wilcoxon rank-sum tests; **p < 0.01, ***p < 0.001; p > 0.05: ns.

(K–O) NSC-specific expression of *mts-DN* results in the increased expression of phosphorylated Akt, as well as a decrease in *ban* activity. (K–L') Brain lobes of control (K and K', *insc-gal4* > *CD8-GFP*) and *mts-DN* (L and L', *insc-gal4* > *CD8-GFP*, *mts-DN*) expressing brains at 6 h ALH. NSCs in green (GFP) and red (Dpn), and pAkt^{S505} (blue). pAkt^{S505} also shown in monochrome; insets showing higher magnifications (K' and L').

(M–O) *ban*-activity sensor, in which a decrease in GFP signal (green) reflects an increase in *ban* activity, in brain lobes of control (M and M') and *mts-DN* expressing brains (N and N') at 6 h ALH. NSCs in red (Dpn) and *mts-DN* (HA-tag, blue). GFP channel also shown in monochrome; insets showing higher magnification (M' and N').

(O) GFP signal (*ban*-activity sensor) quantification in NSCs expressing *mts-DN* normalized to control NSCs (n = 84 *mts-DN* NSCs, 19 BLs, 14 brains; n = 46 control NSCs, 8 BLs, 5 brains; error bars: SEMs; Wilcoxon rank-sum test; **p < 0.01). Anterior up. Scale bars: 10 μm and 17 μm in insets.

(legend continued on next page)

quiescence and proliferation. As in mammals, *Drosophila* NSCs are dependent on niche signals relaying external stimuli for both quiescence and reactivation (Tian et al., 2018; Chaker et al., 2016). In response to a nutritional cue, niche glia cells activate InR/PI3K/Akt signaling in NSCs to promote reactivation (Sousa-Nunes et al., 2011; Chell and Brand, 2010). Niche glia cells also contribute to quiescence by maintaining Hippo signaling activation in NSCs (Ding et al., 2016). In mammals, the insulin and insulin-like growth factor pathway also plays a major role in adult NSC reactivation (Renault et al., 2009; Kippin et al., 2005; Arsenijevic et al., 2001), and while regulation of the Hippo pathway has not yet been implicated in this process, Hippo signaling maintains liver progenitors in quiescence and is indispensable for skin and intestinal regeneration (Wang et al., 2017; Zhou et al., 2009). Here, we show that Mob4, Cka, and PP2A phosphatase, identified in our transcriptome analysis, regulate NSC quiescence to reactivation states, and we propose that they function as an intrinsic integration mechanism of InR/PI3K/Akt and Hippo signals.

We detected the catalytic subunit of PP2A, Mts, downregulated at the transcript level in reactivating versus quiescent NSCs. Mts maintains NSCs in quiescence, preventing premature phosphorylation of Akt, a key component of the InR/PI3K/Akt signaling cascade. PP2A substrate specificity depends on the choice from a variety of regulatory subunits (Shi et al., 2016). In *Drosophila*, the regulatory subunit Wdb was shown to physically interact and negatively regulate Akt in ovaries (Vereshchagina et al., 2008), and has also been implicated in the inhibition of insulin signaling, controlling organism growth and metabolic regulation (Fischer et al., 2015). Wdb orthologs in *Caenorhabditis elegans* (PPTR1) and mammals (B56 β) also dephosphorylate Akt to modulate InR/PI3K/Akt, indicating a conserved role (Rodgers et al., 2011; Padmanabhan et al., 2009). We demonstrate that the inhibition of Mts or of Wdb leads to similar premature NSC reactivation effects, suggesting that Wdb/Mts function together to maintain quiescence. PP2A has been linked to cellular quiescence in different contexts. In the developing *Drosophila* eye and wing, PP2A/Wdb contributes to a quiescent state upon terminal cell differentiation (Sun and Buttitta, 2015); in cycling human cells, PP2A is also required for stable quiescence, a function that is dependent on the B56 γ subunit (Naetar et al., 2014). Thus, PP2A may also have an evolutionary conserved function in maintaining quiescence in NSCs, modulating the InR/PI3K/Akt signaling cascade. PP2A is a pleiotropic phosphatase. In proliferating *Drosophila* NSCs, it contributes to apical-basal polarity and prevents excess self-renewal at later larval stages. Here, Wdb was shown to play no role and instead Twins, a B55 subunit ortholog, regulated PP2A/Mts action (Chabu and Doe, 2009; Krahn et al., 2009; Ogawa et al., 2009; Wang et al., 2009).

In contrast to Mts, we found that Mob4 and Cka upregulated in reactivating versus quiescent NSCs. Both are scaffold proteins

of STRIPAK, a large molecular complex that is highly conserved from fungi to humans containing PP2A (Shi et al., 2016). We demonstrate that the loss of Mob4 or Cka impairs NSC reactivation, while their overexpression can accelerate it. Furthermore, ectopic expression of human Mob4 also induced premature NSC size growth and mitosis entry, suggesting a conserved function. In cultured S2 cells, Mob4 was shown to focus spindle fibers during mitosis (Trammell et al., 2008). Our Mob4 analysis in NSCs exposed a function in cell size growth before mitosis and additionally showed that MbNSCs, which do not enter quiescence, continue dividing in the absence of Mob4, indicating that the role of Mob4 in NSC reactivation is independent of that reported in spindle fibers.

STRIPAK/PP2A associates with Hippo in *Drosophila* and mammalian cells, and restricts *Drosophila* Hippo kinase activity via dephosphorylation (Liu et al., 2016; Couzens et al., 2013; Ribeiro et al., 2010). Previous reports revealed cross-talk inhibition between Hippo and InR/PI3K/Akt pathways in both mammalian and *Drosophila* tissues (Straßburger et al., 2012; Tumaneng et al., 2012). We demonstrate that Mob4 and Cka are both required for the physical association of Mts to Hippo and its subsequent inhibition, as reported (Ribeiro et al., 2010). We also show that upon loss of Mob4, the Hippo pathway consistently remains switched on in NSCs, and InR/PI3K/Akt signaling is inhibited. Finally, we determined that the inhibition of Mts can enhance Hippo signaling in NSCs but that the effect is overcome by premature activation of InR/PI3K/Akt, resulting in earlier NSC reactivation, despite Hippo activity. Our data suggest that as the levels of STRIPAK members Mob4 and Cka increase in NSCs, a complex with Hippo kinase assembles recruiting PP2A/Mts protein to inactivate Hippo signaling. This may function as an intrinsic molecular switch to turn off Hippo signaling and allow the InR/PI3K/Akt cascade to turn on (Figure 6P). Given their large and versatile composition, it is not surprising that STRIPAK complexes are assigned to an increasing number of functions and linked to clinical conditions, including autism and cancer (Shi et al., 2016). It will be important to determine whether and how STRIPAK proteins contribute to regulating the reactivation of other stem cells.

STAR★METHODS

Detailed methods are provided in the online version of this paper and include the following:

- KEY RESOURCES TABLE
- CONTACT FOR REAGENT AND RESOURCES SHARING
- EXPERIMENTAL MODEL AND SUBJECT DETAILS
 - *Drosophila* strains and husbandry
 - S2R+ cell culture, transfection and drug treatment
- METHOD DETAILS
 - NSC transcriptome analysis
 - Immunohistochemistry and EdU incorporation

(P) A model of action of STRIPAK Mob4/Cka/PP2A members: in quiescent NSCs, Mob4 and Cka levels are low, while PP2A (Mts/Wdb) phosphatase targets Akt, ensuring that InR/PI3K/Akt signaling is maintained switched off. Hippo signaling is active (Ding et al., 2016; Poon et al., 2016). Mob4 and Cka levels increase, promoting NSC size growth and entry into division; both are required to direct Mts to switch off Hippo signaling, while the InR/PI3K/Akt cascade becomes active (Sousa-Nunes et al., 2011; Chell and Brand, 2010).

- Image acquisition and processing
- dsRNA synthesis
- Co-immunoprecipitations and western blotting
- QUANTIFICATION AND STATISTICAL ANALYSIS
- DATA AND SOFTWARE AVAILABILITY

SUPPLEMENTAL INFORMATION

Supplemental Information can be found online at <https://doi.org/10.1016/j.celrep.2019.05.023>.

ACKNOWLEDGMENTS

We thank FlyChip (Cambridge Systems Biology Centre, University of Cambridge, UK) and the Bloomington *Drosophila* Stock Center for their services. We are very grateful to those that kindly provided antibodies, fly lines, and plasmids (indicated in Method Details). We also thank Bettina Fisher, Steve Russell, and Matthias Futschik for helpful discussions. This work was supported by the Leverhulme Trust (ECF2010/0526), the BBSRC (BB/M004392/1), the DFG (BE4278/1-1), the Johannes Gutenberg University, Germany, and the Faculty of Medicine and Dentistry, University of Plymouth, UK.

AUTHOR CONTRIBUTIONS

All of the authors designed and performed the experiments. J.G.-R. and C.S.B. wrote the manuscript.

DECLARATION OF INTERESTS

The authors declare no competing interests.

Received: October 13, 2018

Revised: April 14, 2019

Accepted: May 3, 2019

Published: June 4, 2019

SUPPORTING CITATIONS

The following references appear in the Supplemental Information: Berger et al., 2012; Kohyama-Koganeya et al., 2008; Zitserman et al., 2012.

REFERENCES

Arsenijevic, Y., Weiss, S., Schneider, B., and Aebischer, P. (2001). Insulin-like growth factor-I is necessary for neural stem cell proliferation and demonstrates distinct actions of epidermal growth factor and fibroblast growth factor-2. *J. Neurosci.* *21*, 7194–7202.

Baillat, G., Moqrich, A., Castets, F., Baude, A., Bailly, Y., Benmerah, A., and Monneron, A. (2001). Molecular cloning and characterization of phocein, a protein found from the Golgi complex to dendritic spines. *Mol. Biol. Cell* *12*, 663–673.

Berger, C., Harzer, H., Burkard, T.R., Steinmann, J., van der Horst, S., Laursen, A.S., Novatchkova, M., Reichert, H., and Knoblich, J.A. (2012). FACS purification and transcriptome analysis of drosophila neural stem cells reveals a role for Klumpfuss in self-renewal. *Cell Rep.* *2*, 407–418.

Bolstad, B.M., Irizarry, R.A., Astrand, M., and Speed, T.P. (2003). A comparison of normalization methods for high density oligonucleotide array data based on variance and bias. *Bioinformatics* *19*, 185–193.

Bossing, T., and Technau, G.M. (1994). The fate of the CNS midline progenitors in *Drosophila* as revealed by a new method for single cell labelling. *Development* *120*, 1895–1906.

Bossing, T., Barros, C.S., Fischer, B., Russell, S., and Shepherd, D. (2012). Disruption of microtubule integrity initiates mitosis during CNS repair. *Dev. Cell* *23*, 433–440.

Brennecke, J., Hipfner, D.R., Stark, A., Russell, R.B., and Cohen, S.M. (2003). bantam encodes a developmentally regulated microRNA that controls cell proliferation and regulates the proapoptotic gene hid in *Drosophila*. *Cell* *113*, 25–36.

Britton, J.S., and Edgar, B.A. (1998). Environmental control of the cell cycle in *Drosophila*: nutrition activates mitotic and endoreplicative cells by distinct mechanisms. *Development* *125*, 2149–2158.

Britton, J.S., Lockwood, W.K., Li, L., Cohen, S.M., and Edgar, B.A. (2002). *Drosophila*'s insulin/PI3-kinase pathway coordinates cellular metabolism with nutritional conditions. *Dev. Cell* *2*, 239–249.

Cavallucci, V., Fidaleo, M., and Pani, G. (2016). Neural Stem Cells and Nutrients: Poised Between Quiescence and Exhaustion. *Trends Endocrinol. Metab.* *27*, 756–769.

Chabu, C., and Doe, C.Q. (2009). Twins/PP2A regulates aPKC to control neuroblast cell polarity and self-renewal. *Dev. Biol.* *330*, 399–405.

Chaker, Z., Codega, P., and Doetsch, F. (2016). A mosaic world: puzzles revealed by adult neural stem cell heterogeneity. *Wiley Interdiscip. Rev. Dev. Biol.* *5*, 640–658.

Chell, J.M., and Brand, A.H. (2010). Nutrition-responsive glia control exit of neural stem cells from quiescence. *Cell* *143*, 1161–1173.

Chen, H.W., Marinissen, M.J., Oh, S.W., Chen, X., Melnick, M., Perrimon, N., Gutkind, J.S., and Hou, S.X. (2002). CKA, a novel multidomain protein, regulates the JUN N-terminal kinase signal transduction pathway in *Drosophila*. *Mol. Cell. Biol.* *22*, 1792–1803.

Cheung, T.H., and Rando, T.A. (2013). Molecular regulation of stem cell quiescence. *Nat. Rev. Mol. Cell Biol.* *14*, 329–340.

Chintapalli, V.R., Wang, J., and Dow, J.A. (2007). Using FlyAtlas to identify better *Drosophila melanogaster* models of human disease. *Nat. Genet.* *39*, 715–720.

Codega, P., Silva-Vargas, V., Paul, A., Maldonado-Soto, A.R., Deleo, A.M., Pastrana, E., and Doetsch, F. (2014). Prospective identification and purification of quiescent adult neural stem cells from their in vivo niche. *Neuron* *82*, 545–559.

Couzens, A.L., Knight, J.D., Kean, M.J., Teo, G., Weiss, A., Dunham, W.H., Lin, Z.Y., Bagshaw, R.D., Sicheri, F., Pawson, T., et al. (2013). Protein interaction network of the mammalian Hippo pathway reveals mechanisms of kinase-phosphatase interactions. *Sci. Signal.* *6*, rs15.

Ding, R., Weynans, K., Bossing, T., Barros, C.S., and Berger, C. (2016). The Hippo signalling pathway maintains quiescence in *Drosophila* neural stem cells. *Nat. Commun.* *7*, 10510.

Fischer, P., La Rosa, M.K., Schulz, A., Preiss, A., and Nagel, A.C. (2015). Cyclin G Functions as a Positive Regulator of Growth and Metabolism in *Drosophila*. *PLoS Genet.* *11*, e1005440.

Fukada, S., Uezumi, A., Ikemoto, M., Masuda, S., Segawa, M., Tanimura, N., Yamamoto, H., Miyagoe-Suzuki, Y., and Takeda, S. (2007). Molecular signature of quiescent satellite cells in adult skeletal muscle. *Stem Cells* *25*, 2448–2459.

Hamaratoglu, F., Willecke, M., Kango-Singh, M., Nolo, R., Hyun, E., Tao, C., Jafar-Nejad, H., and Halder, G. (2006). The tumour-suppressor genes NF2/Merlin and Expanded act through Hippo signalling to regulate cell proliferation and apoptosis. *Nat. Cell Biol.* *8*, 27–36.

Hannus, M., Feiguin, F., Heisenberg, C.P., and Eaton, S. (2002). Planar cell polarization requires *Widerborst*, a B' regulatory subunit of protein phosphatase 2A. *Development* *129*, 3493–3503.

Hansson, E.M., Teixeira, A.I., Gustafsson, M.V., Dohda, T., Chapman, G., Meletis, K., Muhr, J., and Lendahl, U. (2006). Recording Notch signaling in real time. *Dev. Neurosci.* *28*, 118–127.

Hu, Y., Flockhart, I., Vinayagam, A., Bergwitz, C., Berger, B., Perrimon, N., and Mohr, S.E. (2011). An integrative approach to ortholog prediction for disease-focused and other functional studies. *BMC Bioinformatics* *12*, 357.

Huang, J., and Wang, H. (2018). Hsp83/Hsp90 Physically Associates with Insulin Receptor to Promote Neural Stem Cell Reactivation. *Stem Cell Reports* *11*, 883–896.

- Ito, K., and Hotta, Y. (1992). Proliferation pattern of postembryonic neuroblasts in the brain of *Drosophila melanogaster*. *Dev. Biol.* *149*, 134–148.
- Janssens, V., and Goris, J. (2001). Protein phosphatase 2A: a highly regulated family of serine/threonine phosphatases implicated in cell growth and signaling. *Biochem. J.* *353*, 417–439.
- Kippin, T.E., Martens, D.J., and van der Kooy, D. (2005). p21 loss compromises the relative quiescence of forebrain stem cell proliferation leading to exhaustion of their proliferation capacity. *Genes Dev.* *19*, 756–767.
- Kohyama-Koganeya, A., Kim, Y.J., Miura, M., and Hirabayashi, Y. (2008). A *Drosophila* orphan G protein-coupled receptor BOSS functions as a glucose-responding receptor: loss of boss causes abnormal energy metabolism. *Proc. Natl. Acad. Sci. USA* *105*, 15328–15333.
- Krahn, M.P., Egger-Adam, D., and Wodarz, A. (2009). PP2A antagonizes phosphorylation of Bazooka by PAR-1 to control apical-basal polarity in dividing embryonic neuroblasts. *Dev. Cell* *16*, 901–908.
- Lai, S.L., and Doe, C.Q. (2014). Transient nuclear Prospero induces neural progenitor quiescence. *eLife*. <https://doi.org/10.7554/eLife.03363>.
- Lee, T., and Luo, L. (1999). Mosaic analysis with a repressible cell marker for studies of gene function in neuronal morphogenesis. *Neuron* *22*, 451–461.
- Levy, P., and Larsen, C. (2013). Odd-skipped labels a group of distinct neurons associated with the mushroom body and optic lobe in the adult *Drosophila* brain. *J. Comp. Neurol.* *527*, 3716–3740.
- Li, S., Wang, C., Sandanaraj, E., Aw, S.S., Koe, C.T., Wong, J.J., Yu, F., Ang, B.T., Tang, C., and Wang, H. (2014). The SCFSlimb E3 ligase complex regulates asymmetric division to inhibit neuroblast overgrowth. *EMBO Rep.* *15*, 165–174.
- Li, S., Koe, C.T., Tay, S.T., Tan, A.L.K., Zhang, S., Zhang, Y., Tan, P., Sung, W.K., and Wang, H. (2017). An intrinsic mechanism controls reactivation of neural stem cells by spindle matrix proteins. *Nat. Commun.* *8*, 122.
- Liu, B., and Bossing, T. (2016). Single neuron transcriptomics identify SRSF/SR protein B52 as a regulator of axon growth and Choline acetyltransferase splicing. *Sci. Rep.* *6*, 34952.
- Liu, B., Zheng, Y., Yin, F., Yu, J., Silverman, N., and Pan, D. (2016). Toll Receptor-Mediated Hippo Signaling Controls Innate Immunity in *Drosophila*. *Cell* *164*, 406–419.
- Livak, K.J., and Schmittgen, T.D. (2001). Analysis of relative gene expression data using real-time quantitative PCR and the 2(-Delta Delta C(T)) Method. *Methods* *25*, 402–408.
- Llorens-Bobadilla, E., Zhao, S., Baser, A., Saiz-Castro, G., Zwadlo, K., and Martin-Villalba, A. (2015). Single-Cell Transcriptomics Reveals a Population of Dormant Neural Stem Cells that Become Activated upon Brain Injury. *Cell Stem Cell* *17*, 329–340.
- Macaulay, I.C., and Voet, T. (2014). Single cell genomics: advances and future perspectives. *PLoS Genet.* *10*, e1004126.
- Martynoga, B., Mateo, J.L., Zhou, B., Andersen, J., Achimastou, A., Urbán, N., van den Berg, D., Georgopoulou, D., Hadjir, S., Wittbrodt, J., et al. (2013). Epigenomic enhancer annotation reveals a key role for NFIX in neural stem cell quiescence. *Genes Dev.* *27*, 1769–1786.
- Naetar, N., Soundarapandian, V., Litovchick, L., Goguen, K.L., Sablina, A.A., Bowman-Colin, C., Sicinski, P., Hahn, W.C., DeCaprio, J.A., and Livingston, D.M. (2014). PP2A-mediated regulation of Ras signaling in G2 is essential for stable quiescence and normal G1 length. *Mol. Cell* *54*, 932–945.
- Ogawa, H., Ohta, N., Moon, W., and Matsuzaki, F. (2009). Protein phosphatase 2A negatively regulates aPKC signaling by modulating phosphorylation of Par-6 in *Drosophila* neuroblast asymmetric divisions. *J. Cell Sci.* *122*, 3242–3249.
- Otsuki, L., and Brand, A.H. (2019). Dorsal-Ventral Differences in Neural Stem Cell Quiescence Are Induced by p57(KIP2)/Dacapo. *Dev. Cell* *49*, 293–300.e3.
- Padmanabhan, S., Mukhopadhyay, A., Narasimhan, S.D., Tesz, G., Czech, M.P., and Tissenbaum, H.A. (2009). A PP2A regulatory subunit regulates C. elegans insulin/IGF-1 signaling by modulating AKT-1 phosphorylation. *Cell* *136*, 939–951.
- Poon, C.L., Mitchell, K.A., Kondo, S., Cheng, L.Y., and Harvey, K.F. (2016). The Hippo Pathway Regulates Neuroblasts and Brain Size in *Drosophila melanogaster*. *Curr. Biol.* *26*, 1034–1042.
- Prokop, A., and Technau, G.M. (1991). The origin of postembryonic neuroblasts in the ventral nerve cord of *Drosophila melanogaster*. *Development* *111*, 79–88.
- Renault, V.M., Rafalski, V.A., Morgan, A.A., Salih, D.A., Brett, J.O., Webb, A.E., Villeda, S.A., Thekkat, P.U., Guillerrey, C., Denko, N.C., et al. (2009). FoxO3 regulates neural stem cell homeostasis. *Cell Stem Cell* *5*, 527–539.
- Ribeiro, P.S., Josué, F., Wepf, A., Wehr, M.C., Rinner, O., Kelly, G., Tapon, N., and Gstaiger, M. (2010). Combined functional genomic and proteomic approaches identify a PP2A complex as a negative regulator of Hippo signaling. *Mol. Cell* *39*, 521–534.
- Ritchie, M.E., Phipson, B., Wu, D., Hu, Y., Law, C.W., Shi, W., and Smyth, G.K. (2015). limma powers differential expression analyses for RNA-sequencing and microarray studies. *Nucleic Acids Res.* *43*, e47.
- Rodgers, J.T., Vogel, R.O., and Puigserver, P. (2011). Clk2 and B56 β mediate insulin-regulated assembly of the PP2A phosphatase holoenzyme complex on Akt. *Mol. Cell* *41*, 471–479.
- Schulte, J., Sepp, K.J., Jorquera, R.A., Wu, C., Song, Y., Hong, P., and Littleton, J.T. (2010). DMob4/Phocein regulates synapse formation, axonal transport, and microtubule organization. *J. Neurosci.* *30*, 5189–5203.
- Shi, Z., Jiao, S., and Zhou, Z. (2016). STRIPAK complexes in cell signaling and cancer. *Oncogene* *35*, 4549–4557.
- Snaith, H.A., Armstrong, C.G., Guo, Y., Kaiser, K., and Cohen, P.T. (1996). Deficiency of protein phosphatase 2A uncouples the nuclear and centrosome cycles and prevents attachment of microtubules to the kinetochore in *Drosophila* microtubule star (mts) embryos. *J. Cell Sci.* *109*, 3001–3012.
- Sousa-Nunes, R., Yee, L.L., and Gould, A.P. (2011). Fat cells reactivate quiescent neuroblasts via TOR and glial insulin relays in *Drosophila*. *Nature* *471*, 508–512.
- Spéder, P., and Brand, A.H. (2014). Gap junction proteins in the blood-brain barrier control nutrient-dependent reactivation of *Drosophila* neural stem cells. *Dev. Cell* *30*, 309–321.
- Straßburger, K., Tiebe, M., Pinna, F., Breuhahn, K., and Teleman, A.A. (2012). Insulin/IGF signaling drives cell proliferation in part via Yorkie/YAP. *Dev. Biol.* *367*, 187–196.
- Sun, D., and Butti, L. (2015). Protein phosphatase 2A promotes the transition to G0 during terminal differentiation in *Drosophila*. *Development* *142*, 3033–3045.
- Szklarczyk, D., Franceschini, A., Wyder, S., Forslund, K., Heller, D., Huerta-Cepas, J., Simonovic, M., Roth, A., Santos, A., Tsafou, K.P., et al. (2015). STRING v10: protein-protein interaction networks, integrated over the tree of life. *Nucleic Acids Res.* *43*, D447–D452.
- Takai, A., Murata, M., Torigoe, K., Isobe, M., Mieskes, G., and Yasumoto, T. (1992). Inhibitory effect of okadaic acid derivatives on protein phosphatases. A study on structure-affinity relationship. *Biochem. J.* *284*, 539–544.
- Tian, Z., Zhao, Q., Biswas, S., and Deng, W. (2018). Methods of reactivation and reprogramming of neural stem cells for neural repair. *Methods* *133*, 3–20.
- Trammell, M.A., Mahoney, N.M., Agard, D.A., and Vale, R.D. (2008). Mob4 plays a role in spindle focusing in *Drosophila* S2 cells. *J. Cell Sci.* *121*, 1284–1292.
- Truman, J.W., and Bate, M. (1988). Spatial and temporal patterns of neurogenesis in the central nervous system of *Drosophila melanogaster*. *Dev. Biol.* *125*, 145–157.
- Tsuji, T., Hasegawa, E., and Isshiki, T. (2008). Neuroblast entry into quiescence is regulated intrinsically by the combined action of spatial Hox proteins and temporal identity factors. *Development* *135*, 3859–3869.

- Tumaneng, K., Russell, R.C., and Guan, K.L. (2012). Organ size control by Hippo and TOR pathways. *Curr. Biol.* 22, R368–R379.
- Tung, P.Y., Blischak, J.D., Hsiao, C.J., Knowles, D.A., Burnett, J.E., Pritchard, J.K., and Gilad, Y. (2017). Batch effects and the effective design of single-cell gene expression studies. *Sci. Rep.* 7, 39921.
- Venezia, T.A., Merchant, A.A., Ramos, C.A., Whitehouse, N.L., Young, A.S., Shaw, C.A., and Goodell, M.A. (2004). Molecular signatures of proliferation and quiescence in hematopoietic stem cells. *PLoS Biol.* 2, e301.
- Vereshchagina, N., Ramel, M.C., Bitoun, E., and Wilson, C. (2008). The protein phosphatase PP2A-B' subunit *Widerborst* is a negative regulator of cytoplasmic activated Akt and lipid metabolism in *Drosophila*. *J. Cell Sci.* 121, 3383–3392.
- Virshup, D.M. (2000). Protein phosphatase 2A: a panoply of enzymes. *Curr. Opin. Cell Biol.* 12, 180–185.
- Wang, C., Chang, K.C., Somers, G., Virshup, D., Ang, B.T., Tang, C., Yu, F., and Wang, H. (2009). Protein phosphatase 2A regulates self-renewal of *Drosophila* neural stem cells. *Development* 136, 2287–2296.
- Wang, Y., Yu, A., and Yu, F.X. (2017). The Hippo pathway in tissue homeostasis and regeneration. *Protein Cell* 8, 349–359.
- Weng, L., and Wei, D. (2002). Role of Cka in imaginal disc growth and differentiation. *Drosoph. Inf. Serv.* 85, 8–12.
- Yan, D., Neumüller, R.A., Buckner, M., Ayers, K., Li, H., Hu, Y., Yang-Zhou, D., Pan, L., Wang, X., Kelley, C., et al. (2014). A regulatory network of *Drosophila* germline stem cell self-renewal. *Dev. Cell* 28, 459–473.
- Zheng, Y., Liu, B., Wang, L., Lei, H., Pulgar Prieto, K.D., and Pan, D. (2017). Homeostatic Control of Hpo/MST Kinase Activity through Autophosphorylation-Dependent Recruitment of the STRIPAK PP2A Phosphatase Complex. *Cell Rep.* 21, 3612–3623.
- Zhou, D., Conrad, C., Xia, F., Park, J.S., Payer, B., Yin, Y., Lauwers, G.Y., Thasler, W., Lee, J.T., Avruch, J., and Bardeesy, N. (2009). Mst1 and Mst2 maintain hepatocyte quiescence and suppress hepatocellular carcinoma development through inactivation of the Yap1 oncogene. *Cancer Cell* 16, 425–438.
- Zitserman, D., Gupta, S., Kruger, W.D., Karbowiczek, M., and Roegiers, F. (2012). The TSC1/2 complex controls *Drosophila* pigmentation through TORC1-dependent regulation of catecholamine biosynthesis. *PLoS ONE* 7, e48720.

STAR★METHODS

KEY RESOURCES TABLE

REAGENT or RESOURCE	SOURCE	IDENTIFIER
Antibodies		
Rabbit anti-GFP	Gift from U. Mayor (U. Mayor, personal communication)	N/A
Chicken anti-GFP	Millipore	Cat# 06-896, RRID: AB_310288
Guinea pig anti-Dpn	Gift from J. Knoblich (Levy and Larsen, 2013)	RRID: AB_2314299
Guinea pig anti-Mob4	Gift from T. Littleton (Schulte et al., 2010)	N/A
Mouse anti-Dlg	DSHB	Cat# 4F3 anti-discs large, RRID: AB_528203
Rabbit anti-pH3	Abcam	Cat# ab5176, RRID: AB_304763
Rabbit anti-Cka	Gift from W. Du (Weng and Wei, 2002)	N/A
Rabbit anti-pAKT ^{S505}	CST	Cat# 4054, RRID: AB_331414
Mouse anti-Flag clone M2	Sigma	Cat# F3165, RRID: AB_259529
Rat anti-HA clone 3F10	Roche	Cat# 11867431001, RRID: AB_390919
Rat IgG	Sigma	Cat# I4131, RRID: AB_1163627
Rabbit anti-Akt	CST	Cat# 9272, RRID: AB_329827
Rabbit anti-b-Actin	CST	Cat# 4967, RRID: AB_330288
Mouse anti-Myc clone 9E10	Santa Cruz Biotechnology	Cat# sc-40, RRID: AB_627268
Rabbit anti-pMST1 ^{T183} /pMST2 ^{T180}	CST	Cat# 3681S, RRID: AB_330269
Guinea pig anti-Hippo	Gift from G. Halder (Hamaratoglu et al., 2006)	N/A
Chemicals, Peptides, and Recombinant Proteins		
Okadaic Acid	CST	Cat# 5934
Critical Commercial Assays		
Click-iT EdU Alexa Fluor 594 Imaging Kit	Invitrogen	Cat# C10339
Co-Immunoprecipitation Kit	Pierce	Cat# 26149
Deposited Data		
Transcriptome data	This paper	GEO: GSE128646
Experimental Models: Cell Lines		
<i>D. melanogaster</i> : Cell line S2R+	Gift from B. Houdsen	FlyBase: FBtc0000150
Experimental Models: Organisms/Strains		
<i>D. melanogaster</i> : <i>mob4</i> mutant: y[1] w[*]; Mob4[EYDeltaL3]/CyO	Bloomington Drosophila Stock Center (Schulte et al., 2010)	BDSC: 36331; FlyBase: FBst0036331
<i>D. melanogaster</i> : UAS line expressing <i>mob4</i> RNAi: P{UAS-Mob4.RNAi.JS1}attP2	Bloomington Drosophila Stock Center (Schulte et al., 2010)	BDSC:36488; FlyBase: FBst0036488
<i>D. melanogaster</i> : UAS line expressing <i>mob4</i> : y[1] v[1]; P{y[+7.7] v[+t1.8] = UAS-Mob4.S}attP2	Bloomington Drosophila Stock Center (Schulte et al., 2010)	BDSC: 36329; FlyBase: FBst0036329
<i>D. melanogaster</i> : UAS line expressing <i>hMOB4</i> : y[1] v[1]; P{y[+7.7] v[+t1.8] = UAS-phocein.1}attP2	Bloomington Drosophila Stock Center (Schulte et al., 2010)	BDSC: 36330; FlyBase: FBst0036330
<i>D. melanogaster</i> : UAS line expressing <i>cka-eGFP</i> : w[*]; P{w[+mC] = UASp-Cka.EGFP.C}2	Bloomington Drosophila Stock Center	BDSC: 53756; FlyBase: FBst0053756
<i>D. melanogaster</i> : UAS line expressing <i>wdb-DN</i> : w[*]; P{w[+mC] = UAS-wdb.95-524.HA}6	Bloomington Drosophila Stock Center (Hannus et al., 2002)	BDSC: 55053; FlyBase: FBst0055053
<i>D. melanogaster</i> : UAS line expressing <i>wts</i> RNAi: y[1] sc[*] v[1]; P{y[+7.7] v[+t1.8] = TRiP.GL01331}attP2	Bloomington Drosophila Stock Center (Ding et al., 2016)	BDSC: 41899; FlyBase: FBst0041899

(Continued on next page)

Continued

REAGENT or RESOURCE	SOURCE	IDENTIFIER
<i>D. melanogaster</i> : UAS line expressing <i>hpo</i> RNAi: y[1] v[1]; P{y[+t7.7] v[+t1.8] = TRiP.HMS00006}attP2	Bloomington Drosophila Stock Center (Ding et al., 2016)	BDSC: 33614; FlyBase: FBst0033614
<i>D. melanogaster</i> : UAS line expressing <i>cka</i> RNAi: y[1] v[1]; P{y[+t7.7] v[+t1.8] = TRiP.HM05138}attP2	Bloomington Drosophila Stock Center	BDSC: 28927; FlyBase: FBst0028927
<i>D. melanogaster</i> : Wild type: Oregon-R	Gift from M. Akam (Bossing and Technau, 1994)	FlyBase: FBsn0000276
<i>D. melanogaster</i> : UAS line expressing <i>rheb</i> : w[*]; P{w[+mC] = UAS-Rheb.Pa}3	Gift from R. Sousa-Nunes (Sousa-Nunes et al., 2011)	BDSC: 9689; FlyBase: FBst0009689
<i>D. melanogaster</i> : Gal4 line under the control of <i>grh</i> : <i>Grh-Gal4</i>	Gift from A.H. Brand (Chell and Brand, 2010)	N/A
<i>D. melanogaster</i> : UAS line expressing <i>mts-DN-HA</i> : UAS- <i>mts.dn181-HA</i>	Gift from S. Eaton (Hannus et al., 2002)	N/A
<i>D. melanogaster</i> : line expressing pleckstrin homology domain-GFP fusion protein: <i>PH-GFP</i> (tGPH)	Gift from B. Edgar (Britton and Edgar, 1998)	N/A
<i>D. melanogaster</i> : <i>bantam</i> GFP-sensor line, <i>ban</i> -sensor (<i>db20</i>)	Gift from S.M. Cohen (Brennecke et al., 2003)	N/A
<i>D. melanogaster</i> : <i>mts</i> ^{XE225839} mutant: <i>mts</i> ^{XE2258} /CyO, P{sevRas1.V12}F1 and <i>mts</i> ²⁹⁹ mutant	Gifts from H. Wang (Wang et al., 2009)	BDSC: 5684; FlyBase:FBst0005684 N/A for <i>mts</i> ²⁹⁹
<i>D. melanogaster</i> : Gal4 line under the control of <i>insc</i> : w[*]; P{w[+mW.hs] = GawB}insc[Mz1407]	Bloomington Drosophila Stock Center	BDSC: 8751; FlyBase:FBst0008751
<i>D. melanogaster</i> : Gal4 line under the control of <i>repo</i> : w[1118]; P{w[+m*] = GAL4}repo/TM6, tb	Gift from A. Hidalgo	N/A
<i>D. melanogaster</i> : UAS line expressing <i>CD8-GFP</i> : y[1] w[*]; P{w[+mC] = UAS-mCD8::GFP.L}LL5, P{UAS-mCD8::GFP.L}2	Lee and Luo, 1999	BDSC: 5137; FlyBase:FBst0005137
<i>D. melanogaster</i> : UAS line expressing <i>dicer2</i> : UAS- <i>dicer2</i>	Ding et al., 2016	N/A
Oligonucleotides		
Primer: Anchored polyT AAGCAGTGGTATCAAC GCAGAGTACT ₍₂₆₎ VN	Bossing et al., 2012	N/A
Primer: SM AAGCAGTGGTATCAACGCAGAG TACGCrGrGrG	Bossing et al., 2012	N/A
Primer: Nested AAGCAGTGGTATCAACGCAGAGT	Bossing et al., 2012	N/A
Primers used for RT-qPCR	See Table S4	N/A
dsRNA targeting sequence <i>mob4</i> : Forward: TAATAC GACTCACTATAGGgagatgtggaagtacgacacctg	Schulte et al., 2010	N/A
dsRNA targeting sequence <i>mob4</i> : Reverse: TAATACG ACTCACTATAGGgagatgcgagaagatgcgatacac	Schulte et al., 2010	N/A
dsRNA targeting sequence <i>cka</i> : Forward: TAATACG ACTCACTATAGGgatacgggtccagtctgtgc	This paper	N/A
dsRNA targeting sequence <i>cka</i> : Reverse: TAATACG ACTCACTATAGGgtgttagccaccacgata	This paper	N/A
dsRNA targeting sequence <i>DsRed</i> : Forward: TAATAC GACTCACTATAGGgcccgatgaacttcacctgt	This paper	N/A
dsRNA targeting sequence <i>DsRed</i> : Reverse: TAATAC GACTCACTATAGGgaggagcgtcatcaaggagt	This paper	N/A
Recombinant DNA		
Plasmid: 12XCSL DsRedExpressDL	Hansson et al., 2006	Addgene plasmid #47683
Plasmid: Flag-NTAN	Gift from P. Ribeiro (Ribeiro et al., 2010)	N/A

(Continued on next page)

Continued

REAGENT or RESOURCE	SOURCE	IDENTIFIER
Plasmid: Flag-Hippo	Gift from P. Ribeiro (Ribeiro et al., 2010)	N/A
Plasmid: Myc-Mts	Gift from P. Ribeiro (Ribeiro et al., 2010)	N/A
Plasmid: HA-Mts	Gift from P. Ribeiro (Ribeiro et al., 2010)	N/A
Plasmid: Myc-Akt	Gift from W. Hongyan (Li et al., 2014)	N/A
Software and Algorithms		
R/Bioconductor Limma	Ritchie et al., 2015	https://bioconductor.org/packages/release/bioc/html/limma.html
STRING v10.5	Szklarczyk et al., 2015	https://string-db.org/cgi/input.pl?sessionId=QMsQ2cmXKFYZ&input_page_show_search=on
FlyAtlas	Chintapalli et al., 2007	http://flyatlas.org/atlas.cgi
DIOPT – DRSC Integrative Ortholog Prediction Tool	Hu et al., 2011	https://www.flyrnai.org/cgi-bin/DRSC_orthologs.pl

CONTACT FOR REAGENT AND RESOURCES SHARING

Further information and requests for resources and reagents should be directed to and will be fulfilled by the Lead Contact, Claudia Barros (claudia.barros@plymouth.ac.uk).

EXPERIMENTAL MODEL AND SUBJECT DETAILS

***Drosophila* strains and husbandry**

Drosophila stocks obtained from the Bloomington *Drosophila* Stock Center are: *mob4^{EYΔL3}* (36331) (Schulte et al., 2010) rebalanced over *CyO*, *P(GAL4-twi.G)2.2*; *UAS-mob4^{RNAi}* (36488) (Schulte et al., 2010); *UAS-mob4* (36329) (Schulte et al., 2010); *UAS-hMOB4* (36330) (Schulte et al., 2010); *UAS-cka-eGFP* (53756); *UAS-wdb-DN* (*UAS-wdb.95-524.HA*; 55053) (Hannus et al., 2002); *UAS-wts^{RNAi}* (41899) (Ding et al., 2016); *UAS-hpo^{RNAi}* (33614) (Ding et al., 2016) and *UAS-cka^{RNAi}* (28927). Other stocks used are: Wild-type *Oregon-R* (kind gift from M. Akain); *UAS-rheb* (Blomington 9689) (Sousa-Nunes et al., 2011) (kind gift from R. Sousa-Nunes); *grh-Gal4* (Chell and Brand, 2010) (kind gift from A.H. Brand); *UAS-mts-DN* (*UAS-mts.dn181-HA*) (Hannus et al., 2002) (kind gift from S. Eaton); *PH-GFP* (tGPH) (Britton and Edgar, 1998) (kind gift from B. Edgar); *ban-sensor* (*db20*) (Brennecke et al., 2003) (kind gift from S.M. Cohen), *mts²⁹⁹* and *mts^{XE2258}* (Wang et al., 2009) (kind gifts from H. Wang). NSC-specific RNAi and overexpression assays were performed using *insc-Gal4* (*w¹¹¹⁸*; *p{GAWB}inscMZ1407*) and glial-specific expression assays used *repo-Gal4* (*w¹¹¹⁸*; *p{GAWB}repo/TM6b*, *iab-lacZ*). *grh-Gal4* driver was recombined with *UAS-CD8-GFP*. For rescue experiments, *insc-Gal4* and *repo-Gal4* drivers were recombined or combined with the *mob4^{EYΔL3}* mutant strain. For other assays, the *insc-Gal4* driver was recombined with *UAS-CD8-GFP* and/or combined with *UAS-dicer2* (Ding et al., 2016). Fly lines were kept in standard *Drosophila* fly food. Egg collections and larvae rearing were performed on agar juice plates (21 g agar, 200ml of grape juice per l of water) supplemented with yeast paste. Egg lays were collected in either 30min or 1h time-windows. For nutritional deprivation experiments, freshly hatched larvae were transferred to agar plates prepared with amino-acid free media (5% sucrose, 1% agar in phosphate buffered saline, PBS).

S2R+ cell culture, transfection and drug treatment

S2R+ cells (kind gift from B. Houdsen) were maintained in 25- or 75-cm² T-flasks at 25°C in Schneider's Medium (GIBCO) with 10% heat-inactivated FBS (One Shot, GIBCO) and antibiotics. For transient transfections, 1.6x10⁶ cells/well were seeded in 6-well plates. Effectene transfection reagent (Quiagen) was used to transfect 1 μg and/or 2 μg of each appropriate plasmid and/or dsRNA, respectively, following manufacturer guidelines. Cells were incubated 72 hours before harvest. Plasmids used are Flag-NTAN, Flag-Hippo, Myc-Mts, HA-Mts (kind gifts from P. S. Ribeiro) and Myc-AKT (kind gift from W. Hongyan). For okadaic acid experiments, cells were transfected as above, incubated 70 hours and treated with 50 nM okadaic acid (CST) or 0.005% DMSO (vehicle; Corning) for 2 hours prior harvest.

METHOD DETAILS

NSC transcriptome analysis

Single NSC harvest, mRNA isolation, cDNA generation and microarray hybridization were performed essentially as previously described (Bossing et al., 2012). Single quiescent (small; 4–5 μm) and reactivating (enlarged) NSCs were individually removed from freshly dissected 17 ALH CNS expressing membrane-tagged GFP specifically in NSCs (*grh-Gal4, UAS-CD8-GFP*). Samples with any trace of non-fluorescent material were rejected. Each single cell was expelled in its own Eppendorf tube containing annealing mix: 0.3 μL anchored polyT primer (5'-AAGCAGTGGTATCAACGCAGAGTACT₍₂₆₎VN-3', 10pM), 0.3 μL SM primer (5'-AAGCAGTGGTATCAACGCAGAGTACGCrGrGrG-3', 10pM), 0.4 μL RNase inhibitor (Superase, Ambion) and 2 μL Lysis Mix (10% Nonidet P-40, 0.1M DTT in DEPC-treated ultrapure water), and processed in less than 20 min. Each sample was spun (14000rpm, 1min, 4°C), primers annealed (3min, 70°C) and snap-frozen in dry ice/ isopropanol. 1.5 μL of mix 1 (1 μL Invitrogen first strand buffer, 0.5 μL 10mM dNTPs) and 0.5 μL of mix 2 (3 μL Invitrogen Superscript II reverse transcriptase, 0.5 μL Ambion Superase RNase inhibitor) were added per sample. Samples were thawed during centrifugation (14000rpm, 1 min, 4°C) and reverse transcribed (37°C, 90min), followed by enzyme thermal inactivation (65°C, 10 min). RNA was digested in 2 μL digestion mix (0.7 μL Roche RNase H buffer, 0.5 μL Roche RNase H, 0.8 μL ultrapure water) for 20min at 37°C, followed by enzyme thermal inactivation (65°C, 15 min). For cDNA PCR amplification, 2 μL of nested primer (5'-AAGCAGTGGTATCAACGCAGAGT-3'), 2 μL dNTPs (10mM), 5 μL Roche buffer, 0.5 μL Roche Long Expand polymerase and 34.5 μL of ultrapure water were added. PCR program: one cycle (95°C 3min, 50°C 5min, 68°C 15min) followed by 25 cycles (95°C 20 s, 60°C 1min, 68°C 7min). 3 pairs of NSC quiescent/ reactivating samples showing clear banding patterns on agarose gels were sent for microarray analysis (FlyChip, University of Cambridge). 1 μg of each sample were Klenow-labeled using BioPrime DNA Labeling System (Invitrogen) in the presence of Cy3- or Cy5-dCTP (GE Healthcare) for 2 hours 37°C. Unincorporated dye and nucleotides were removed using AutoSeq G-50 columns (GE Healthcare), following manufacturer instructions. Cy3- and Cy5-labeled pairs of samples were combined with salmon sperm DNA as blocking agent and co-hybridized (16 hours, 51°C) in a HybStation hybridization station (Digilab Genomic Solutions) on long oligonucleotides FL003 microarrays (International *Drosophila* Array Consortium; Gene Expression Omnibus accession number GPL14121). Post-hybridization washes were performed according to Full Moon Biosystems protocols. Detailed protocols for labeling, hybridization and washing can be requested from the Cambridge Systems Biology Centre UK (<https://www.sysbiol.cam.ac.uk/CSBC>). Arrays were scanned at 5 μm resolution (GenePix scanner, Axon Instruments) using optimized PMT gain settings for each channel.

RT-qPCR validation of selected genes was done using SYBRGreen on a StepOnePlus thermal cycler (Applied Biosystems) and primers indicated in Table S4. *ribosomal protein 49 (rp49)* was used as internal calibrator for all reactions. Single NSC cDNA samples used were obtained as described above. Candidates validated were also selected based on their Gene Ontology (GO) *Nervous system development* and *Neurogenesis* classification (STRING v10.5) (Szklarczyk et al., 2015).

Tissue-specific expression of identified targets was performed using FlyAtlas (Chintapalli et al., 2007). Gene orthology analysis used DIOPT (DRSC Integrative Ortholog Prediction Tool) (Hu et al., 2011). Protein-protein interaction network of *Drosophila* PP2A-STRIPAK components was performed using STRING (v10.5) (Szklarczyk et al., 2015) with experimental-based data only as source, and as previously described (Zheng et al., 2017; Liu et al., 2016; Ribeiro et al., 2010).

Immunohistochemistry and EdU incorporation

Immunohistochemistry assays were performed as previously described (Chell and Brand, 2010), with minor modifications. Briefly, larval CNSs were dissected in PBS and fixed for 20 min in 4% formaldehyde/PBS with 5 μM MgCl₂ and 0.5 μM EGTA or 10 μM MgCl₂ and 1 μM EGTA (3rd instar larvae), followed by washes in PBS (2 × 10 min, 3 rinses between washes) and block for 1h in PBST (PBS, 1% Triton X-100) with 10% fetal bovine serum (FBS). Primary antibodies were incubated in PBST overnight or for 2 nights at 4°C. CNSs were washed in PBST and secondary antibodies incubated 2h at room temperature, followed by PBST washes and sequentially embedding in 50% and 70% glycerol before mounting in a 1:1 mix of 70% glycerol and Vectashield (Vector Laboratories). Antibodies used are: rabbit anti-GFP (1:1000, kind gift from U. Mayor), chicken anti-GFP (1:500, Millipore), guinea pig anti-Dpn (1:2000, kind gift from J. Knoblich), guinea pig anti-Mob4 (1:1000, kind gift from T. Littleton), mouse anti-Dlg (1:50, DSHB), rabbit anti-pH3 (1:1000, Abcam), rabbit anti-Cka (1:1000, kind gift from W. Du), rabbit anti-pAKT^{S505} (1:50, CST) and rat anti-HA clone 3F10 (1:1000, Roche). EdU incorporation assays were performed as previously described (Sousa-Nunes et al., 2011). Briefly, CNSs were dissected in PBS and incubated in 10 μM EdU/PBS for 1h at room temperature. CNSs were fixed for 15min in 4% formaldehyde/PBS and incorporated EdU detected using Click-iT EdU Imaging kit following manufacturer instructions (Invitrogen).

Image acquisition and processing

Images were obtained on a Leica SP8 confocal laser-scanning microscope using LAS X software. Quantifications were made using z stacks of 1.5 μm step size, comprising whole brain lobes, VNCs or CNSs. Representative images shown are single optical sections, with the exception of Figure 1A, which is a z-projection stack (3 steps, 0.5 μm each), and EdU incorporations, which are z-projection stacks encompassing whole CNSs. Images were processed in Fiji v2.0 or Adobe Photoshop CS6 and assembled in Adobe Illustrator CS6. NSC sizes (maximum diameters) (Chell and Brand, 2010), pH3 scorings, Mob4 and Cka signal intensities (pixel intensity/ NSC maximum area), *ban*-GFP signal intensity (pixel intensity/ NSC maximum area outlined by Dpn staining) and EdU voxel quantification were performed using Fiji v2.0 or Adobe Photoshop CS6.

dsRNA synthesis

For *cka*, *mob4* and *DsRed* dsRNA, DNA templates of target genes were PCR amplified from larval genomic DNA or 12XCSL-DsRedExpressDL plasmid (Addgene) to include the T7 promoter sequence on both ends. Primers used are: dsRNAmob4_Fwd: 5'-TAATACGACTCACTATAGGGGagatgtggaagtagcagcacctg-3' (Schulte et al., 2010), dsRNAmob4_Rev: 5'-TAATACGACTCACTA TAGGGagatgtagcagaagatgtagcagcac-3' (Schulte et al., 2010), dsRNAcka_Fwd: 5'-TAATACGACTCACTATAGGGGatagcgggtccagtctgtgc-3', dsRNAcka_Rev: 5'-TAATACGACTCACTATAGGGGtgtgttagccaccacgata-3', dsRNADsRed_Fwd: 5'-TAATACGACTCACTA TAGGGgcccgatgaacttcacctgt-3', dsRNADsRed_Rev:

5'-TAATACGACTCACTATAGGGGcaggagcgtcatcaaggagt-3'. The size of DNA bands was confirmed, purified using QIAquick Gel Extraction Kit (QIAGEN) and used as template for dsRNA synthesis. *In vitro* transcriptions were performed using MEGAscript T7 kit (Invitrogen), incubated for 6 hours at 37°C and treated with TURBO DNase (Invitrogen) for 15 min at 37°C. RNA was precipitated using LiCl precipitation solution (Invitrogen) and re-hydrated in ultrapure water. dsRNA was annealed by incubation at 65°C 30 min and cooled down to room temperature.

Co-immunoprecipitations and western blotting

S2R+ cells were harvested and lysed in lysis buffer (25mM Tris, 0.15M NaCl, 1mM EDTA, 1% NP-40, 5% glycerol; pH 7.4) supplemented with protease inhibitor (Complete, EDTA-free; Sigma) and phosphatase inhibitors (cocktails B+C; Santa Cruz Biotechnology). Cell extracts were spun at 14000 rpm for 30 min at 4°C and proteins quantified (BCA protein assay, Pierce). Using the Pierce Co-immunoprecipitation kit (Pierce), 20 µg of anti-Flag M2 (Sigma), anti-HA (3F10; Roche), or rat IgG (Sigma) were immobilized in 50 µL of AminoLink Plus Coupling resin slurry following manufacturer instructions. Protein lysates were incubated in the resin on a rotator at 4°C overnight, washed 4 times with PBS and eluted following manufacturer instructions. Detection of proteins was performed using standard SDS-PAGE and western blotting using ECL or ECL Plus chemiluminescent substrate (Pierce). Antibodies used are: rabbit anti-Akt (1:500, CST), rabbit anti-pAkt^{S505} (1:500, CST), rabbit anti-β-Actin (1:1000, CST), mouse anti-Flag clone M2 (1:3000, Sigma), mouse anti-Myc clone 9E10 (1:500, Santa Cruz Biotechnology), rabbit anti-Cka (1:5000, kind gift from W. Du), guinea pig anti-Mob4 (1:5000, kind gift from T. Littleton), rabbit anti-pMST1^{T183}/pMST2^{T180} (1:500, CST), guinea pig anti-Hippo (1:5000, kind gift from G. Halder) and rat anti-HA clone 3F10 (1:3000, Roche).

QUANTIFICATION AND STATISTICAL ANALYSIS

Transcriptome data: all genes with raw signal intensity values below 150 were removed from the analysis, generating a matrix containing 2455 genes. Quantile normalization (Bolstad et al., 2003) across all samples was performed using R/Bioconductor limma package (Ritchie et al., 2015). Remaining genes were analyzed with limma, by fitting a linear model. Adjusting *p-values* with False Discovery Rate (FDR) did not reach statistical significance. Instead, a limma moderated paired t test was employed. Targets with expression fold changes with associated *p* < 0.05 values were used for subsequent analysis, including expression validation. Expression of selected candidate genes assayed by RT-qPCR was quantified using the Livak method (Livak and Schmittgen, 2001).

Other statistics were performed using SigmaPlot Version 12.5 (Systat software): Shapiro-Wilk and equal variance tests used to evaluate normality; Student's t test applied when data fitted a normal distribution; Wilcoxon rank-sum test used for non-parametric data; *p* < 0.05 considered significant. Data from *Drosophila in vivo* assays were obtained from a minimum of two biological replica sets; sample numbers are indicated in figure legends. Cell culture/ biochemistry results derive from a minimum of three independent assays. Histograms show mean ± standard error of the mean. Boxplots represent 25th and 75th percentiles, black line indicates median, red line specifies mean, whiskers indicate 10th and 90th percentiles.

DATA AND SOFTWARE AVAILABILITY

Processed transcriptome data is shown in Table S1. Raw transcriptome data has been deposited in the Gene Expression Omnibus (GEO) public database under ID code GSE128646.

Cell Reports, Volume 27

Supplemental Information

STRIPAK Members Orchestrate Hippo and Insulin

Receptor Signaling to Promote

Neural Stem Cell Reactivation

Jon Gil-Ranedo, Eleanor Gonzaga, Karolina J. Jaworek, Christian Berger, Torsten Bossing, and Claudia S. Barros

Supplemental Figures and Figure Text

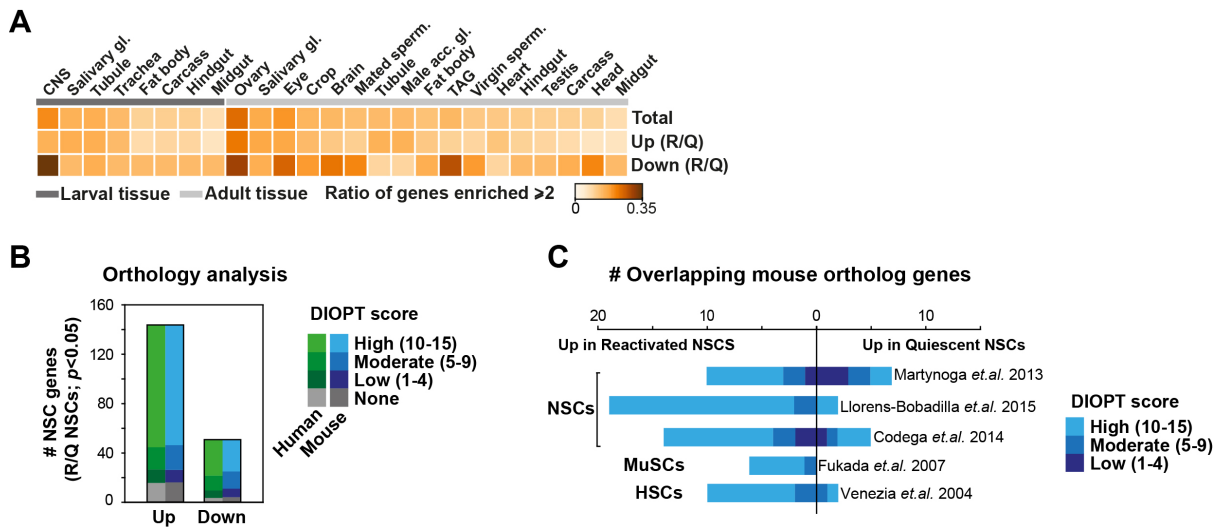


Figure S1, related to Figure 1. Tissue expression enrichment and orthology conservation of identified targets in transcriptome analysis. (A) Heatmap depicting identified larval and adult tissue-specific gene sets enriched by a minimum of 2-fold to expression in whole fly. gl: gland. Sperm: spermatheca; acc: accessory; TAG: thoracoabdominal ganglion. See also Table S2. **(B)** Number of human and mouse orthologues (single best matches) of identified genes grouped by orthology score (DIOPT) (Hu, et al., 2011). See also Table S1. **(C)** Number of identified genes with mouse orthologues (single best matches) reported upregulated in quiescent or proliferating mouse embryonic or adult NSCs, skeletal muscle satellite stem cells (MuSCs) and hematopoietic stem cells (HSC). DIOPT score groups indicated. See also Table S3. The data used for the above assays comprise targets identified in our transcriptome analysis as up- or downregulated in reactivating (R) versus quiescent (Q) NSCs (limma moderated t -test, $p < 0.05$).

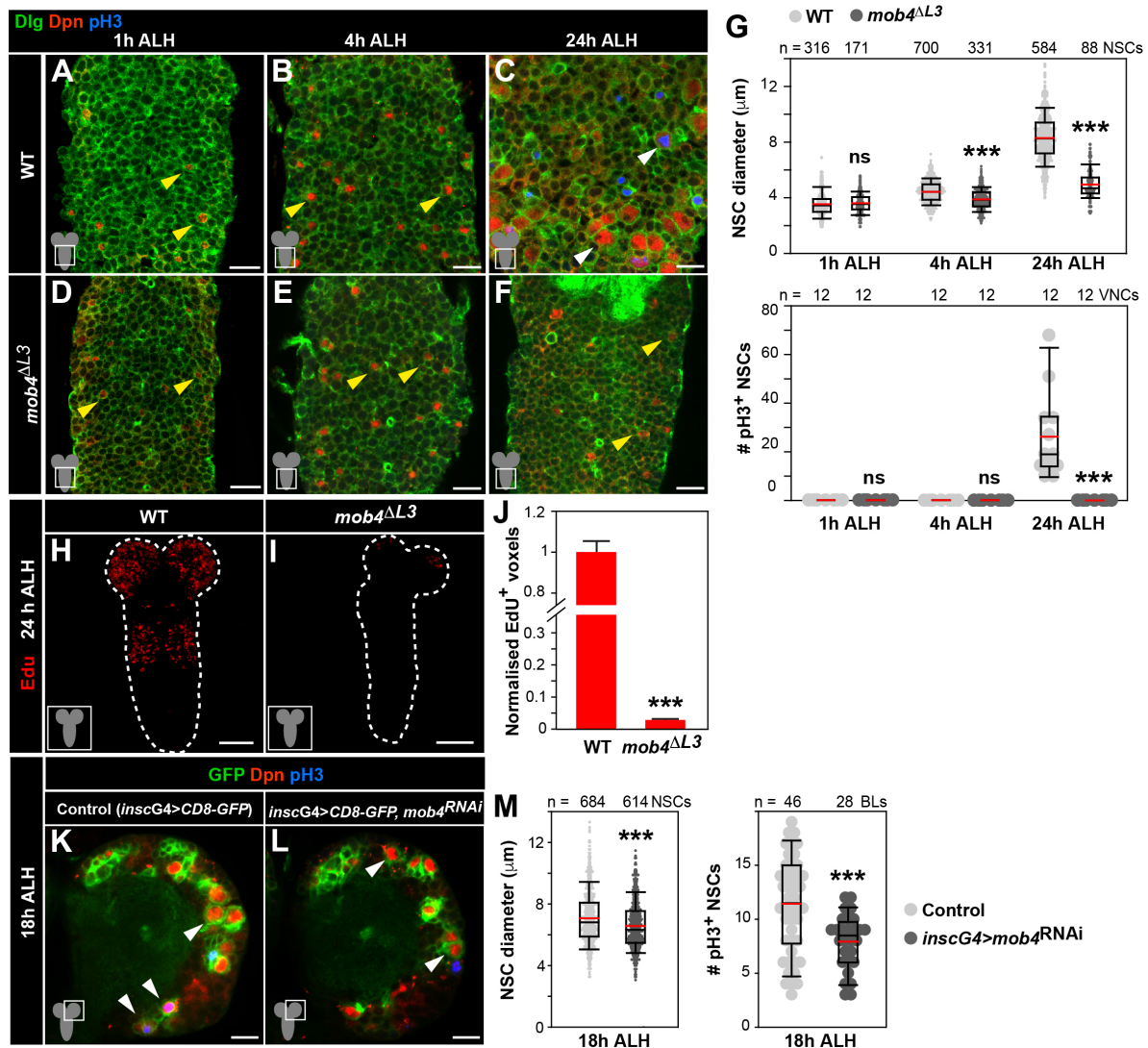


Figure S2, related to Figure 2. NSC reactivation defects upon *Mob4* loss or inhibition. (A-G) NSC enlargement and division is impaired in *mob4* mutant ventral nerve cords (VNCs). VNCs of WT (A, 1h ALH; B, 4h ALH; C, 24h ALH) and *mob4*^{ΔL3} (D, 1h ALH; E, 4h ALH; F, 24h ALH). NSCs in red (Dpn), cell membranes in green (Dlg), divisions in blue (pH3). Yellow and white arrowheads indicate quiescent and reactivated NSC examples, respectively. Scale bar: 10μm. Anterior up. (G) Quantification of NSC diameters (1h ALH: WT n=316 NSCs, 7 VNCs; *mob4*^{ΔL3} n=171 NSCs, 5 VNCs. 4h ALH: WT n=700 NSCs, 6 VNCs; *mob4*^{ΔL3} n=331 NSCs, 5 VNCs. 24h ALH: WT n=584 NSCs, 5 VNCs; *mob4*^{ΔL3} n=88 NSCs, 8 VNCs) and proliferation (1h ALH: WT n=12 VNCs; *mob4*^{ΔL3} n=12 VNCs. 4h ALH: WT n=12 VNCs; *mob4*^{ΔL3} n=12 VNCs. 24h ALH: WT n=12 VNCs; *mob4*^{ΔL3} n=12 VNCs). (H-J) NSCs in *mob4* mutant larval brains do not enter S-phase, except the MbNSCs. WT (H) and *mob4*^{ΔL3} (I) CNSs at 24hph Edu-labelled (red). (J) Quantification of Edu⁺

voxels from CNSs, normalized to controls (WT n=7 CNSs, *mob4*^{ΔL3} n=8 CNSs; error bars: s.e.m). Scale bar: 50μm. (K-M) NSC-specific expression of *mob4*-RNAi results in a small reduction in cell size and decreased number of NSCs in division. Brain lobes (BLs) of control (K, *insc-gal4>CD8-GFP*) and *mob4*-RNAi expressing brains (L, *insc-gal4> CD8-GFP, mob4*^{RNAi}) at 18h ALH. NSCs in green (*CD8-GFP*, GFP) and red (Dpn), divisions in blue (pH3). Arrowheads: NSC examples. Anterior up. Scale bar: 10μm. (M) Quantification of NSC diameters (*insc-gal4>CD8-GFP*, n=684 NSCs, 9 BLs, 9 brains; *insc-gal4> CD8-GFP, mob4*^{RNAi} n=614 NSCs, 8 BLs, 8 brains) and divisions (*insc-gal4>CD8-GFP*, n=46 BLs, 23 brains; *insc-gal4> CD8-GFP, mob4*^{RNAi} n=28 BLs, 14 brains). Wilcoxon rank sum tests, ****p*<0.001, *p*>0.05: non-significant (ns).

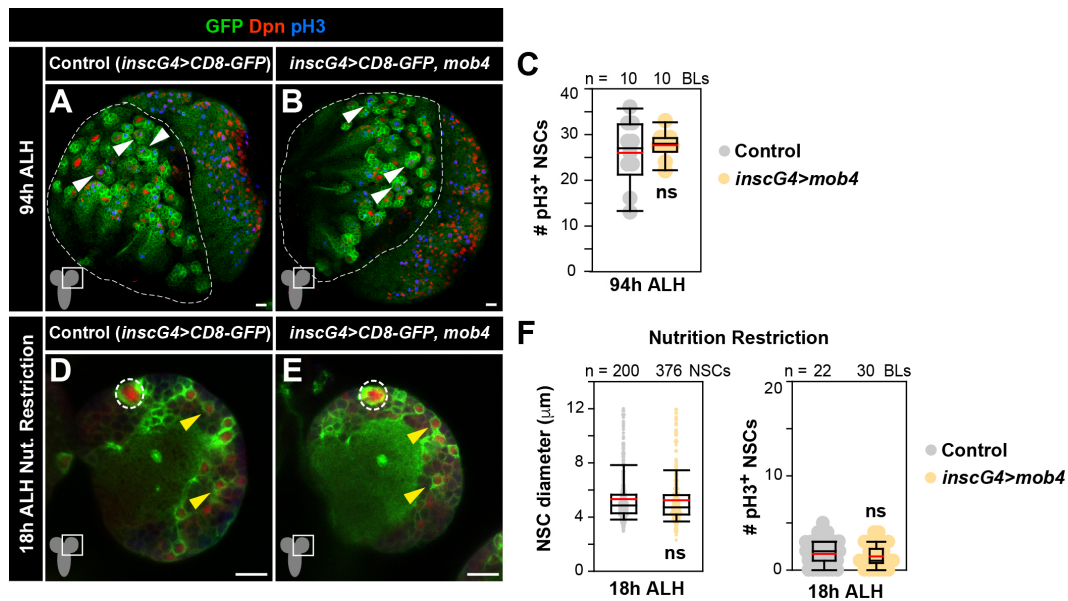


Figure S3, related to Figure 3. *Mob4* overexpression does not lead to NSC overproliferation nor induces NSC reactivation under nutrition restriction.

NSC-specific *mob4* overexpression does not affect NSC proliferation in late larval brains (A-C) nor promotes reactivation of NSCs in larvae deprived of amino acids (sucrose-only diet; D-F). Brain lobes (BLs) of control (A, D, *insc-gal4>CD8-GFP*) and *mob4* overexpressing brains (B, E, *insc-gal4>CD8-GFP, mob4*) at 94h (A, B) and 18h ALH (D, E). NSCs in green (GFP) and red (Dpn), divisions in blue (pH3). Dashed line: central brain region. White arrowheads: dividing NSC examples. Yellow arrowheads: quiescent NSC examples. Dashed circles: MbNSCs. Scale bar: 10 μ m. Anterior up. (C) Quantification of NSC divisions (94h ALH: *insc-gal4>CD8-GFP* n=10 BLs, 10 brains; *insc-gal4>CD8-GFP, mob4* n=10 BLs, 10 brains). (F) Quantification of NSC diameters (18h ALH: *insc-gal4>CD8-GFP* n=200 NSCs, 6 BLs, 5 brains; *insc-gal4>CD8-GFP, mob4* n=376 NSCs, 5 BLs, 5 brains) and divisions (18h ALH: *insc-gal4>CD8-GFP* n=22 BLs, 16 brains; *insc-gal4>CD8-GFP, mob4* n=30 BLs, 16 brains). Wilcoxon rank sum tests, $p>0.05$: non-significant (ns).

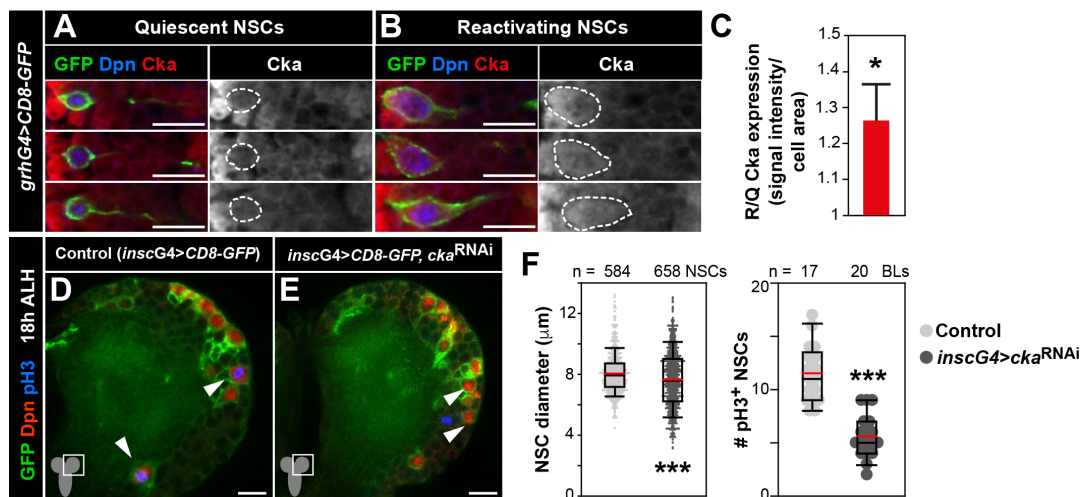


Figure S4, related to Figure 5. Cka inhibition delays NSC growth and division.

(A-C) Cka is upregulated in reactivating (R) compared with quiescent (Q) NSCs. Examples of quiescent (small; A) and reactivating (enlarged, B) NSCs in 17h ALH brains (VNC thoracic region) labelled with *grh-Gal4* driving *CD8-GFP* (GFP, green), Cka (red) and Dpn (blue). Cka channel also shown in monochrome. Dashed lines: cell bodies. (C) Cka protein quantification in reactivating normalised to quiescent NSCs (n= 20 reactivating NSCs and n=20 quiescent NSCs, 20 BLs, 10 brains; error bars: s.e.m.; Wilcoxon rank sum test, * $p < 0.05$). (D-F) NSC-specific expression of *cka-RNAi* results in reduced cell size and decreased number of NSCs in division. Brain lobes (BLs) of control (D, *insc-gal4>CD8-GFP*) and *cka-RNAi* expressing brains (E, *insc-gal4> CD8-GFP, cka^{RNAi}*) at 18h ALH. NSCs in green (*CD8-GFP*, GFP) and red (Dpn), divisions in blue (pH3). Arrowheads: NSC examples. Anterior up. Scale bar: 10 μ m. (F) Quantification of NSC diameters (*insc-gal4>CD8-GFP*, n=584 NSCs, 8 BLs, 4 brains; *insc-gal4> CD8-GFP, cka^{RNAi}* n=658 NSCs, 8 BLs, 4 brains) and divisions (*insc-gal4>CD8-GFP*, n=17 BLs, 9 brains; *insc-gal4> CD8-GFP, cka^{RNAi}* n=20 BLs, 10 brains). Wilcoxon rank sum tests, *** $p < 0.001$.

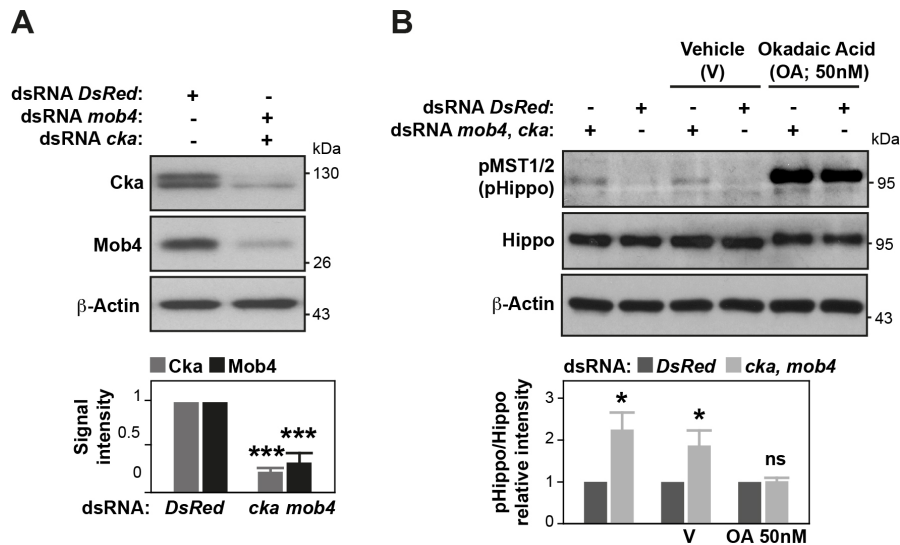


Figure S5, related to Figure 5. Inhibition of Mob4 and Cka increase Hippo phosphorylation. (A) Efficiency of *mob4* and *cka* RNAi-mediated depletions used in *Drosophila* S2R+ assays. dsRNAs targeting *mob4* or *cka*, but not *DsRed* control, lead to depletion of Mob4 and Cka proteins. Lysates analysed with indicated antibodies. β -Actin: loading control. Quantification of Mob4 and Cka signal intensities normalised to control (*DsRed* RNAi) levels (lower panel; n=3 independent assays; error bars: s.e.m; Student's *t*-tests, *** $p < 0.001$). (B) Mob4/ Cka depletion leads to increased levels of activated (phosphorylated) Hippo (pHippo) in S2R+ cells, consistent with published studies (Zheng, et al., 2017; Liu, et al., 2016; Ribeiro, et al., 2010). *Drosophila* S2R+ cells treated with dsRNAs targeting *mob4* and *cka* or control *DsRed*, as well as in the presence of vehicle (0.0005% DMSO) or Okadaic acid (OA) as a positive control for hippo phosphorylation. Lysates analysed by western-blot with indicated antibodies. β -Actin: loading control. Note the total Hippo band mobility shift due to hyperphosphorylation in OA-treated samples. Quantification of pHippo levels shown as mean of the ratio between pHippo and total Hippo signal intensities relative to control (*DsRed* RNAi) levels (lower panel; n=3 independent assays; error bars: s.e.m; Student's *t*-tests, $p^* < 0.05$, $p > 0.05$: non-significant, ns).

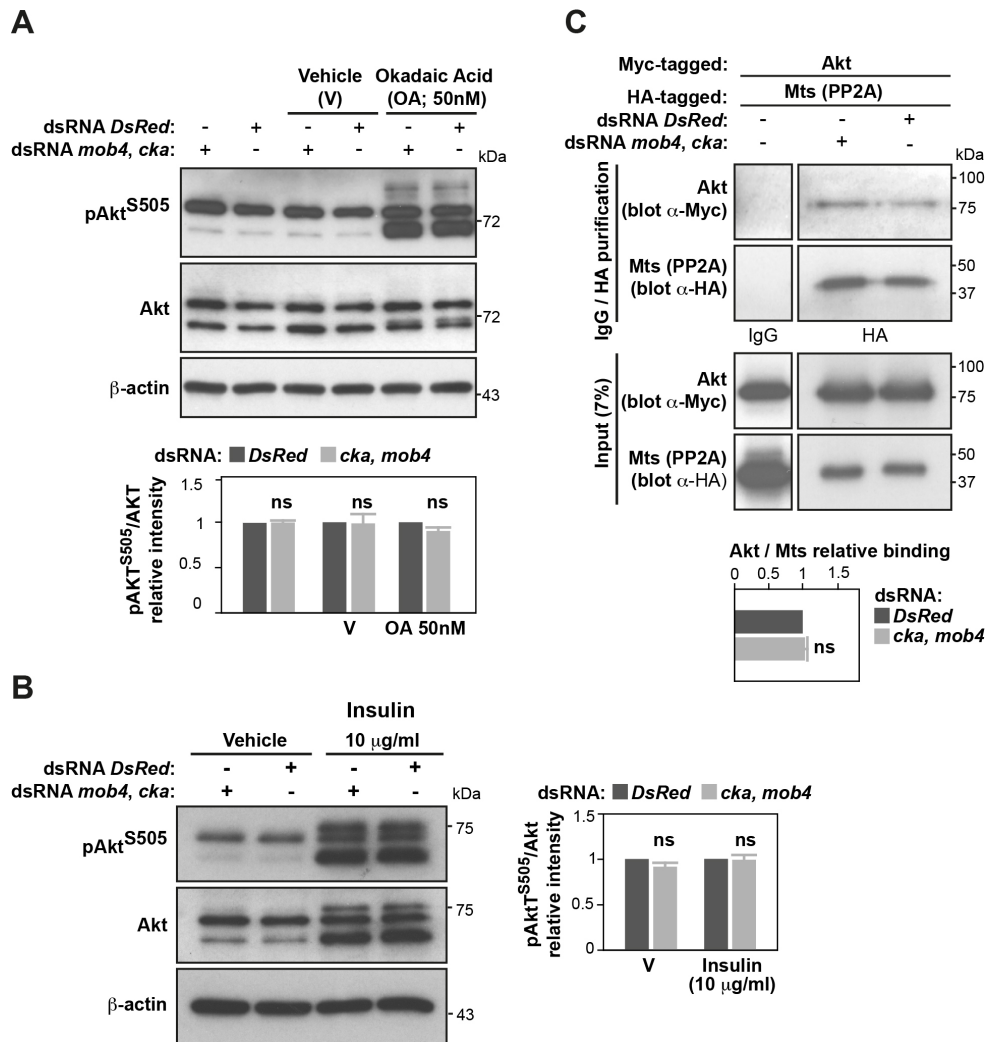


Figure S6, related to Figure 5. Inhibition of Mob4 and Cka does not affect Akt phosphorylation nor the association of PP2A/Mts to Akt. (A, B) Depletion of *mob4* and *cka* has no effect in the levels of activated (phosphorylated) Akt (pAkt^{S505}) in S2R+ cells (A) with or without stimulation with Insulin (B). (A) *Drosophila* S2R+ cells treated with dsRNAs targeting *mob4* and *cka* or control *DsRed*, as well as in the presence of Okadaic acid (OA) as a positive control for Akt phosphorylation or vehicle (V). Lysates analysed with indicated antibodies. β-Actin: loading control. Quantification of pAkt levels shown as mean of the ratio between pAkt and total Akt signal intensities relative to control (*DsRed* RNAi) levels (lower panel; n=3 independent assays). (B) RNAi-mediated depletion of *mob4* and *cka*, or control *DsRed*, in S2R+ cells treated with Insulin or vehicle. Lysates analysed by western-blot with indicated antibodies. β-Actin: loading control. Quantification of pAkt levels shown as mean of pAkt/ Akt signal intensity ratios relative to control (*DsRed* RNAi) levels (right panel; n=3 independent assays). (C) Co-IP assays using S2R+ cells

expressing Myc-Akt and HA-Mts, in addition to RNAi against *mob4* and *cka* or control *DsRed*. Lysates and HA-purified immunoprecipitates analysed by western-blot with indicated antibodies. Negative control co-IP performed using rat IgG instead of rat anti-HA antibody. Quantification of relative binding of Myc-Akt to HA-Mts shown as mean of the ratio between Myc-Akt and HA-Mts signal intensities relative to control (*DsRed* RNAi) levels (lower panel; n=3 independent assays). Error bars: s.e.m. Wilcoxon rank-sum tests, $p>0.05$: non-significant (ns).

Supplemental Table

Gene (Symbol)	Forward Primer (5'→3')	Reverse Primer (5'→3')	Source
<i>ase</i>	CACCTACCAACTGCTGACG	GCTGCTGCTGCTAATGTTG	This paper
<i>dpn</i>	CGCTATGTAAGCCAAATGGATGG	CTATTGGCACACTGGTTAAGATGG	(Berger, et al., 2012)
<i>rheb</i>	TGAGGTGGTGAAGATCATATACGAA	GCCAGCTTCTTGCCTTCCT	(Zitserman, et al., 2012)
<i>cka</i>	GGAGACGGAAGGCGTCAT	TCTCGTCGTCGGACATC	This paper
<i>CG10903</i>	GAGTCTCGGTTGATTTTGGACA	TCTCCAGAATGACATCCCCA	This paper
<i>asf1</i>	GGGCGACACATCTTTGTCTTC	GCAGGTAAGCAGAACAATGGTAA	This paper
<i>Gbeta13F</i>	TGGTGGCTATCTATCGTGCTG	GCCCCAAAACGAGGTTACCTG	This paper
<i>phax</i>	ATGATGGAAGTGCACGCAAT	CAGGTGGTAAGGGGACTGG	This paper
<i>NiPp1</i>	ATGGCTAACAGCTACGACATACC	TGTTGCGACCAAATAGATAGCAT	This paper
<i>mob4</i>	TGGGCACGATCAGATTCTCC	CATCTTCTCGCACGCTACT	This paper
<i>crc</i>	GAAACTGGGAGGATACGTGG	GAGAGGTCTGAATGCCTTTGTC	This paper
<i>bet3</i>	ATGTCACGACAAGCCTCTCG	GAGTGCTCCGTAGGTGAGT	This paper
<i>ed</i>	GATGAGCTCCTGTTCTCCGG	GTTGGAATCGCAATGGTCGG	This paper
<i>pdp1</i>	AATCCCATTACCAGCGCAA	GGCATTCCCATTGATCCCT	This paper
<i>how</i>	AACTTTGTCCGGTCGCATTTT	CGTCCTCCTTCTTCTTGTCG	This paper
<i>p120ctn</i>	AACATGGACCTTTTATTGACGC	ATATCCTGCTGCCGAAAATTGA	This paper
<i>Rip11</i>	TGGAGTCCGACGCACTGTA	CAATGGTGACGAAGCAGTTGT	This paper
<i>l(2)35Df</i>	CATCGAAAGAAGCTACATCCTCC	GTGGGTTTCGTCATCTGCATTAT	This paper
<i>nito</i>	ACAAGAAGTTTGGCGATTTTAGC	CTTCAGGCGTTTCGGAAGCAA	This paper
<i>mts</i>	TCCAGTTCATAAGAGCCGC	CACGATCGCAATGTGGTCAC	This paper
<i>rp49</i> (calibrator)	GCTAAGCTGTCCGACAAATG	GTTCGATCCGTAACCGATGT	(Kohyama-Koganeya, et al., 2008)

Table S4, related to STAR Methods. Primers used for real-time quantitative PCR assays.